

Supporting Information Appendix

Structural basis for specific ligation of the peroxisome proliferator-activated receptor δ

Chyuan-Chuan Wu^{a,b,1}, Thomas J. Baiga^{a,b,1}, Michael Downes^{c,1}, James J. La Clair^{a,b}, Annette R. Atkins^c, Stephane B. Richard^{a,b}, Weiwei Fan^c, Theresa A. Stockley-Noel^{a,b}, Marianne E. Bowman^{a,b}, Joseph P. Noel^{a,b,2}, and Ronald M. Evans^{a,c,2}

^aHoward Hughes Medical Institute, The Salk Institute for Biological Studies, La Jolla, CA 92037; ^bJack H. Skirball Center for Chemical Biology and Proteomics, The Salk Institute for Biological Studies, La Jolla, CA 92037; and ^cGene Expression Laboratory, The Salk Institute for Biological Studies, La Jolla, CA 92037

Author contributions: C.-C.W., T.J.B., M.D., J.J.L., A.R.A., S.B.R., J.P.N., and R.M.E. designed research; C.-C.W., M.D., J.J.L., A.R.A., S.B.R., W.F., T.A.S-N., M.E.B., and J.P.N. performed research; C.-C.W., T.J.B., M.D., J.J.L., A.R.A., S.B.R., W.F., J.P.N., and R.M.E. analyzed data; and C.-C.W., M.D., J.J.L., A.R.A., and J.P.N. wrote the paper.

Conflict of interest statement: J.P.N., T.J.B., M.D., and R.M.E are coinventors of PPAR δ molecules/ligands and methods of use and may be entitled to royalties.

Data deposition: The atomic coordinates and structure factors have been deposited in the Protein Data Bank, www.pdb.org [PDB ID codes 5U3Q, 5U3R, 5U3S, 5U3T, 5U3U, 5U3V, 5U3W, 5U3X, 5U3Y, and 5U3Z (for compounds 1–10•hPPAR δ -LBD complex structures, respectively), 5U40 and 5U41 (for 15 and 16•hPPAR δ -LBD complex structures, respectively), and 5U42, 5U43, 5U44, 5U45, and 5U46 (for 11–14•hPPAR δ -LBD and GW501516•hPPAR δ -LBD complex structures, respectively)].

¹C.-C.W., T.J.B., and M.D. contributed equally to this work.

²To whom correspondence may be addressed. Email: evans@salk.edu or noel@salk.edu.

A. Experimental Methods and Materials

A.1. Protein expression and purification. The coding sequence for hPPAR δ -LBD (base pairs 508 to 1323) was sub-cloned into the expression vector pHIS8, which produces recombinant protein fused to a N-terminal thrombin-cleavable HIS8-tag (36). *Escherichia coli* BL21 (DE3) harboring the pHIS8-hPPAR δ -LBD plasmid (wild-type or mutated constructs) were grown in 1L of Terrific Broth (TB) medium at 37°C to an OD₆₀₀ of approximately 1.0, then the culture was cooled down to 20°C, and induced with 1 mL of 0.5 M IPTG. Proteins were expressed at 20°C for 16 h. Cells were harvested by centrifuging at 6,000 rpm for 10 min, resuspended with lysis buffer (50 mM Tris-HCl, pH 8.0, 500 mM NH₄OAc, 20 mM imidazole, 1% Tween 20, 10% [v/v] glycerol and 10 mM β -mercaptoethanol), and lysed by sonication on ice. Sonicate was centrifuged at 18,000 rpm for 30 min. The resultant supernatant was loaded onto a 2 mL Ni²⁺-NTA-agarose column. The column was washed with 50 mL wash buffer (50 mM Tris-HCl, pH 8.0, 500 mM NH₄OAc, 20 mM imidazole, 10% [v/v] glycerol and 10 mM β -mercaptoethanol) followed by bound protein elution with (50 mM Tris-HCl, pH 8.0, 500 mM NH₄OAc, 250 mM imidazole, 10% [v/v] glycerol and 10 mM β -mercaptoethanol). Eluted protein was treated with thrombin to remove the HIS₈-tag while dialyzing against the digestion buffer (50 mM Tris-HCl, pH 8.0, 500 mM NaCl and 10 mM β -mercaptoethanol) at 4°C for 16 h. The thrombin-treated protein was loaded onto a 1 mL benzamidine-sepharose column to remove thrombin. Remaining HIS8-tagged protein and non-specifically bound Ni²⁺-NTA agarose-binding proteins were cleared using a 1 mL Ni²⁺-agarose column. Tag-free hPPAR δ -LBD was dialyzed against gel filtration buffer (20 mM HEPES, pH 7.5, 500 mM NH₄OAc and 10 mM DTT) at 4°C for 16 h. Protein was concentrated to 5 mL (~1 mg mL⁻¹) and loaded onto a Superdex 200 size exclusion column. hPPAR δ -LBD eluted near 30 kDa, was collected and pooled, and concentrated to 10 mg mL⁻¹ for protein crystallization, or stored in 50% (v/v) glycerol at -20°C for further experiments.

A.2. Cell culture and C2C12 myoblast assays. C2C12 myoblasts were cultured in DMEM media supplemented with 20% (v/v) FBS and differentiated into myotubes over 5 d in DMEM media supplemented with 2% (v/v) horse serum. Gene expression analyses of PPAR δ target genes involved in fatty acid metabolism including *Angptl4* and *Pdk4* in C2C12 myotubes were measured by quantitative PCR (qPCR). Briefly, myotubes were treated with vehicle (DMSO), GW501516, or compound **9** for 2, 5, 10 or 24 hr at 100 nM final concentrations of ligands. Cells were directly collected in Trizol (Invitrogen), and RNA extracted with the RNeasy Mini kit with on-column DNase treatment (Qiagen). For quantitated RNA expression, 1 μ g of RNA was reverse transcribed using the iScript Supermix (Biorad), and qPCR performed with gene-specific primer pairs shown below in SYBR Green Master Mixes on the CFX384 qPCR system (Biorad). Gene expression results were normalized to the 60S acidic ribosomal protein P0 gene (*Rplp0*).

Primer pairs were designed as shown below:

5'-GATGTCTGTTTCGAACTTTGACC-3' (Pdk4_Forward),
5'-CTGGTGAAGAGCTGGTATATCC-3' (Pdk4_Reverse),
5'-CATCCTGGGACGAGATGAACT-3' (Angptl4_Forward),
5'-TGACAAGCGTTACCACAGGC-3' (Angptl4_Reverse),
5'-TGACATCGTCTTTAAACCCCG-3' (Rplp0_Forward), and
5'-TGTCTGCTCCCACAATGAAG-3' (Rplp0_Reverse).

For Seahorse experiments, C2C12 myoblasts were seeded at a density of 2×10^4 cells per well in XF96 plates and differentiated over 5 d in DMEM media supplemented with 2% (v/v) horse serum. The resultant myotube cultures were then supplemented with vehicle (DMSO), GW501516, or compound **9** at 100 nM final concentrations of ligands and cultured for an additional 15 hr. The differentiated myotubes were then transferred into FAO Assay Medium (111 mM NaCl, 4.7 mM KCl, 1.25 mM CaCl_2 , 2 mM MgSO_4 , 1.2 mM NaH_2PO_4) supplemented with 2.5 mM glucose, 0.5 mM carnitine, and 5 mM Na-HEPES buffer adjusted to pH 7.4 and maintained at 37° C. Oxygen consumption rates (OCRs) were measured using the XF96 platform (Seahorse Biosciences) according to manufacturer's instructions following injection of bovine serum albumin (BSA) or palmitate (PAL) plus BSA (XF proprietary Palmitate-BSA FAO Substrates, Seahorse Biosciences, Part #102720-100) to determine glucose-fueled or fatty acid-fueled respiration, respectively.

A.3. Crystallization, X-ray diffraction data collection and structure determination. The ligand-bound hPPAR δ -LBD crystals were prepared starting with previously published conditions (27). Briefly, purified hPPAR δ -LBD was mixed with respective ligands dissolved in 100% (v/v) DMSO. The final concentration of GW501516 and **1** was 0.75 mM. For the remaining compounds, the final ligand concentrations were 7.5 mM (for **2**, **3**, **8**, **9**, **10**, **11** and **12**), 5.0 mM (for **5**, **6**, **7** and **16**), 2.5 mM (for **4** and **15**), or 5.8 mM (for **13** and **14**). All crystals were grown by using the hanging drop vapor diffusion method at room temperature ($\sim 22^\circ\text{C}$). The initial drops were set up with 3 μL protein-ligand solution mixed with 3 μL reservoir solution (40 mM Bis-Tris propane-HCl, pH 7.5-8.8 200 mM KCl, 4 to 14% [w/v] PEG 8K, 2.5% [v/v] 1,2-propandiol, 1 mM EDTA and 10 mM DTT). Crystals grew for 1 week. For data collection, crystals were transiently soaked with reservoir solution containing 8% (w/v) PEG 8K and 20% (w/v) PEG 1K, and then quickly frozen in liquid nitrogen. X-ray diffraction data was collected at beamlines 8.2.1 or 8.2.2 of the Advanced Light Source (ALS), Lawrence Berkeley National Laboratory. Data for the GW501516-bound crystal were collected at beamline 9-1 of the Stanford Synchrotron Radiation Light Source (SSRL). All data sets were processed with the HKL2000 program suit (54) and scaled with Aimless (55) of the CCP4i program suit (56).

All structures were solved by molecular replacement using the published hPPAR δ -LBD structure as a starting model (PDB ID: 1GWX) (27). The solved structures then underwent cycles of manual model building using Coot (57) and refinement using the PHENIX program suit (58). Figures in this paper were generated using Pymol Version 1.7.4.1 (Schrödinger, LLC).

A.4. Site-direct mutagenesis of hPPAR δ -LBD. To generate point mutations in the ligand-binding pocket of hPPAR δ -LBD, the pHIS8-hPPAT δ -LBD plasmid was used as templates for site-direct mutagenesis. Oligonucleotides (Eurofins) for the method were designed as shown below with the mutation sites underlined:

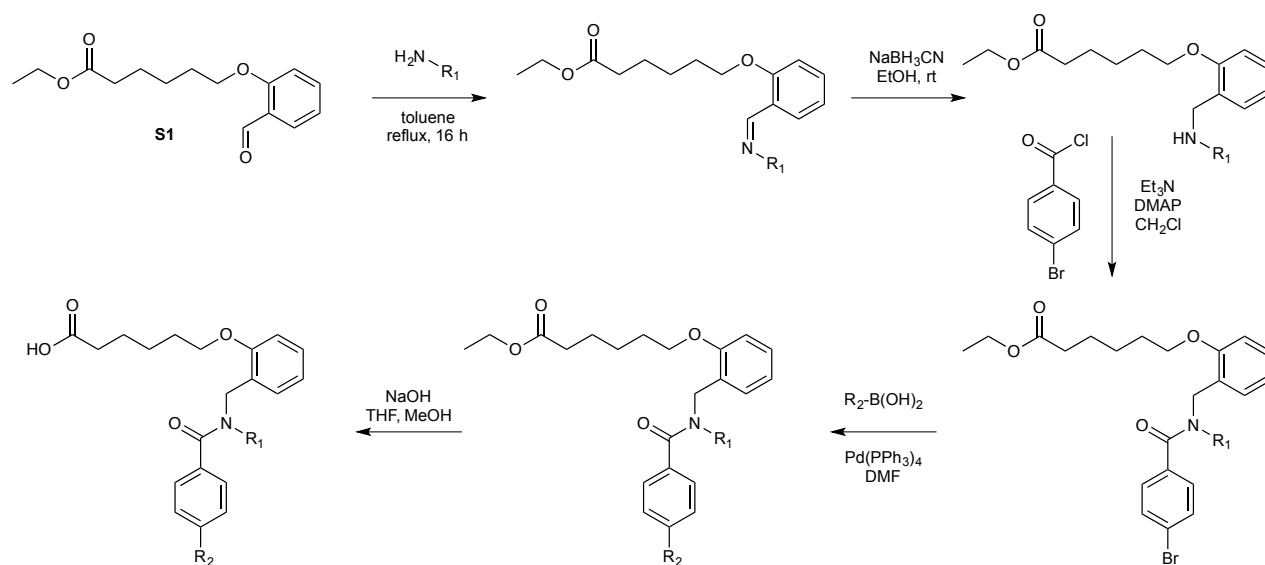
5'-CTCTATCATGAACAAGGACGGGCTGC-3' (V298M_Forward),
5'-CCTTGTTCATGATAGAGGCCAGCATGG-3' (V298M_Reverse),
5'-GACGGGATGCTGGTAGCCAAC-3' (L303M_Forward),
5'-CAGCATCCCGTCCTTGTTGACG-3' (L303M_Reverse),
5'-GGCTTTATGACCCGTGAGTTCCTGCG-3' (V312M_Forward),
5'-CACGGGTCATAAAGCCACTGCCGTTG-3' (V312M_Reverse),
5'-GATATCATGGAGCCTAAGTTTGAATTTG-3' (I328M_Forward), and
5'-GGCTCCATGATATCACTGAAGGG-3' (I328M_Reverse).

A.5. Thermal-shift binding assay. The thermostabilities of hPPAR δ -LBD in the presence of compounds **1-16** or GW501516 were assayed using a ThermoFluor-type assay (35). Briefly, 8 μ L of 2.5 μ M purified wild-type hPPAR δ -LBD, hPPAR δ -LBD V298M, L303M, V312M or I328M mutants were dispensed into 384-well plates (\sim 0.6 μ g protein per well). Compounds **1-16** or GW501516 (in 100% [v/v] DMSO) were serially diluted with DMSO and added into wells (1 μ L for each reaction; final concentration of DMSO 10% [v/v]). Proteins and ligands were then incubated at 4°C for 2 h. A 1 μ L aliquot of 20-fold SYPRO Orange dye (Sigma-Aldrich) was added into each well and then wells were sealed. Dye and protein solutions were mixed by vortexing for 15 s, and spun down at low speed. Protein melting curves were measured using the LightCycler 480 Real-Time PCR System II (Roche) with the following program: 30 s at 20°C, ramp to 85°C at 0.04°C \cdot s⁻¹, 30 s at 20°C, excitation and emission wavelengths 483 nm and 568 nm, respectively. The melting temperatures (T_m s) of the hPPAR δ -LBD wild-type and mutated proteins in the absence of ligands provided the baseline T_m (T_m^0) for each protein. The thermo-shift effects of compounds presented in this study were obtained by plotting mean ΔT_m s ($T_m^{\text{ligand}} - T_m^0$) versus ligand concentration using data from at least three replicate experiments, as listed in Figs. 3B and C and S7. A three-parameter dose-response nonlinear regression function was fit to the data using the GraphPad Prism v5.04 (GraphPad Software, La Jolla, CA). The resultant curves, calculated EC₅₀ values and maximum T_m shifts for each compound are listed in Fig. S6.

A.6. General chemical methods. Chemical reagents were purchased from Acros, Fluka, Sigma-Aldrich, or TCI. Deuterated NMR solvents were purchased from Cambridge Isotope Laboratories. All reactions were conducted with rigorously dried anhydrous solvents obtained by passing through solvent columns composed of activated Al₂O₃ alumina. Anhydrous *N,N*-dimethylformamide was obtained by passage over activated molecular sieves and a subsequent NaOCN column to remove traces of dimethylamine. Triethylamine (Et₃N) was dried over Na and freshly distilled. All reactions were performed under positive pressure Ar in oven-dried glassware sealed with septa, with stirring using Teflon coated stir bars and IKAMAG RCT-basic mechanical stirrers (IKA GmbH). Solutions were heated using either a sand or silicon oil bath. Analytical Thin Layer Chromatography (TLC) was performed on Silica Gel 60 F254 precoated glass plates (EM Sciences). Preparative TLC (pTLC) was conducted on Silica Gel 60 plates (EM Sciences). Visualization was achieved with UV light and/or an appropriate stain (I₂ on SiO₂, KMnO₄, bromocresol green, dinitrophenylhydrazine, ninhydrin, and ceric ammonium molybdate). Flash chromatography was carried out using Geduran Silica Gel 60 (40-63 mesh) from EM Biosciences. Yields and characterization data correspond to isolated, chromatographically, and spectroscopically homogeneous materials. ¹H NMR spectra were recorded on a Varian Innova 500 spectrometer. Chemical shifts for ¹H NMR and ¹³C NMR analyses were referenced using the signal from the residual solvent for ¹H spectra, or to the ¹³C signal from the deuterated solvent. Chemical shift δ values for ¹H and ¹³C spectra are reported in parts per million (ppm) relative to these referenced values, and multiplicities are abbreviated as s = singlet, d = doublet, t = triplet, q = quartet, m = multiplet, br = broad. All ¹³C NMR spectra were recorded with complete proton decoupling. FID files were processed using MestraNova 11.0.1 (MestreLab Research). Electrospray (ESI) mass spectrometric analyses were performed using a ThermoFinnigan LCQ Deca spectrometer, and high-resolution analyses were conducted using a ThermoFinnigan MAT900XL mass spectrometer with electron impact (EI) ionization. A Thermo Scientific LTQ Orbitrap XL mass spectrometer was used for high-resolution electrospray ionization mass spectrometry analyses (HR-ESI-MS). Spectral data and procedures are provided for all new compounds and copies of select spectra are included at the end of the Supplementary Information.

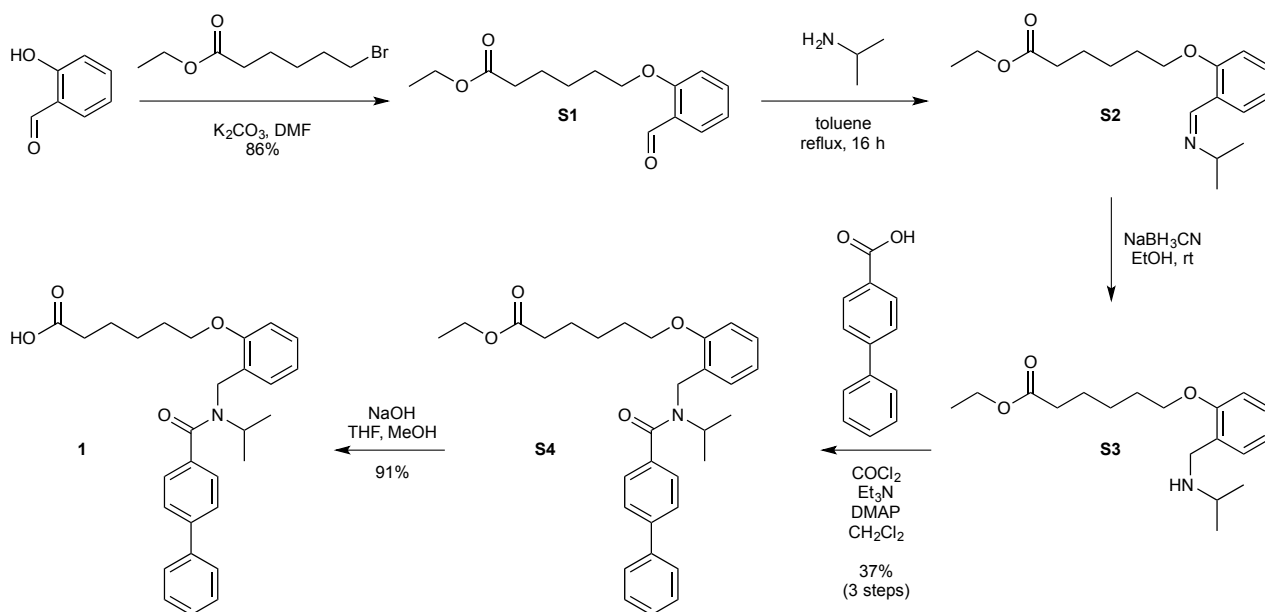
A.7. Panel development and set selection. A panel of over 100 compounds was developed using the motif shown in Fig. 1. Small-scale syntheses scaled at 10-100 mg were deployed in a combinatorial manner without purification between steps using the route depicted in Scheme S1 (59). Crude products at the end of the 5-step processes were subjected to Flash purification on a packed silica gel system (Biotage) to obtain pure materials. The purity of these materials was given at >95% by LC/MS or HPLC analyses. A set of 16 compounds, compounds **1-16** (Fig. 1) were selected from this panel and evaluated in this study.

Compounds **1** and **9** were selected for scale up to complete the work.



Scheme S1. Combinatorial Syntheses. Samples of each compound were prepared at mg scales using split-and-pool methods with structural modifications around two positions: substituent-1 (R_1) and substituent-2 (R_2).

A.8. Preparative synthesis of 1. Compound **1** was prepared in 4 steps in 28% overall yield from intermediate **S1**. Scheme S2 and the following sections describe the methods, materials, and spectral data analyses for intermediates and the final product **1**.



Scheme S2. Synthesis of compound **1**. Preparation of **1** required only two chromatographic purifications as crude **S1** and **S2** could be used without additional purification.

Ethyl 6-(2-formylphenoxy)hexanoate (S1). Salicylaldehyde (5.00 g, 40.92 mmol), was dissolved in DMF (25 mL). Ethyl 6-bromohexanoate (10.92 mL, 61.37 mmol) and anhydrous K₂CO (14.14 g, 102.29 mmol) were added sequentially. The mixture was heated to reflux. After 3 h, the mixture was cooled to rt and H₂O (100 mL) was added. The resulting mixture was extracted with EtOAc (3 × 200 mL), washed with H₂O (100 mL) and satd. NaCl (100 mL), dried over Na₂SO₄, and concentrated on a rotary evaporator. The resulting aldehyde **S1** (9.35 g, 86%) was sufficiently pure (~95%) for the next step. For analytical purposes, pure material was obtained by flash chromatography eluted with a gradient of hexanes to 1:1 hexanes:EtOAc.

Aldehyde **S1**: ¹H NMR (CDCl₃, 500 MHz) δ 10.43 (s, 1H), 7.76 (dd, *J* = 1.9, 7.7 Hz, 1H), 7.46 (ddd, *J* = 1.9, 7.3, 8.5 Hz, 1H), 6.49 (t, *J* = 7.5 Hz, 1H), 6.90 (d, *J* = 7.9 Hz, 1H), 4.06 (q, *J* = 7.1 Hz, 2H), 4.01 (t, *J* = 6.3 Hz, 2H), 2.27 (t, *J* = 7.5 Hz, 2H), 1.81 (qd, *J* = 6.4, 7.8 Hz, 2H), 1.65 (p, *J* = 7.5 Hz, 2H), 1.48 (m, 2H), 1.19 (t, *J* = 7.1 Hz, 3H); ¹³C NMR (CDCl₃, 125 MHz) δ 190.0, 173.7, 161.5, 136.1, 128.4, 125.0, 120.7, 112.5, 68.3, 60.5, 34.3, 28.9, 25.8, 24.8, 14.1; HR-ESI-MS *m/z* calcd. for C₁₅H₂₀O₄ [M+Na]⁺: 287.1254, found 287.1251.

Ethyl 6-(2-((isopropylamino)methyl)phenoxy)hexanoate (S3). Aldehyde **S1** (6.20 g, 23.46 mmol) was dissolved in toluene (50 mL). Isopropylamine (3.36 mL, 39.09 mmol) was added along with 1 M HCl (250 μL). The mixture was brought to reflux over a Dean-Stark trap. We found that the optimal yield of this reaction occurred when adding two additional portions of isopropylamine (3.36 mL, 39.09 mmol) and 1 M HCl (250 μL) at 2 h and 4 h. The reaction was monitored by NMR analyses, as TLC analysis failed to provide accurate readings of imine formation. The reaction was typically complete (>98% conversion) after 6 h. Once complete, the mixture was dried via rotary evaporation, and samples of imine **S2** were used without further purification.

The entire portion of crude imine **S2** (7.16 g) was dissolved in EtOH (100 mL) and cooled to 0°C. NaBH₃CN (1.77 g, 28.15 mmol) was added carefully over 5 min. After 6 h, an additional portion of NaBH₃CN (1.20 g, 19.09 mmol) was added and the mixture stirred overnight. The reaction was neutralized by the addition of H₂O (100 mL). The resulting mixture was extracted with EtOAc (3 × 200 mL), washed with brine (100 mL), dried over Na₂SO₄, and concentrated on a rotary evaporator. The resulting crude amine **S3** (6.92 g, 95%) was sufficiently pure (~95%) for the next step. Alternatively, pure material was obtained by flash chromatography eluted with a gradient of hexanes to 1:2 hexanes:EtOAc.

Intermediate **S3**: ¹H NMR (CDCl₃, 500 MHz) δ 7.36 (dd, *J* = 1.6, 7.4, 1H), 7.32 (dd, *J* = 1.7, 7.9 Hz, 1H), 6.92 (t, *J* = 7.5 Hz, 1H), 6.88 (d, *J* = 8.3 Hz, 1H), 5.29 (s, 1H), 4.10 (q, *J* = 6.5 Hz, 2H), 4.06 (t, *J* = 6.0 Hz, 2H), 4.03 (s, 1H), 2.32 (t, *J* = 7.4 Hz, 2H), 1.86 (p, *J* = 6.9 Hz, 2H), 1.67 (h, *J* = 7.6 Hz, 2H), 1.49 (m, 2H), 1.27 (d, *J* = 6.6 Hz, 2H), 1.24 (t, *J* = 7.2 Hz, 3H); ¹³C NMR (CDCl₃, 125 MHz) δ 173.9, 157.1, 131.9, 131.3, 121.0, 118.9, 111.4, 68.1, 60.5, 50.8, 45.1, 34.2, 28.8, 25.6,

24.6, 19.3, 14.3; HR-ESI-MS m/z calcd. for $C_{18}H_{29}NO_2$ $[M+H]^+$: 308.2220, found 308.2219.

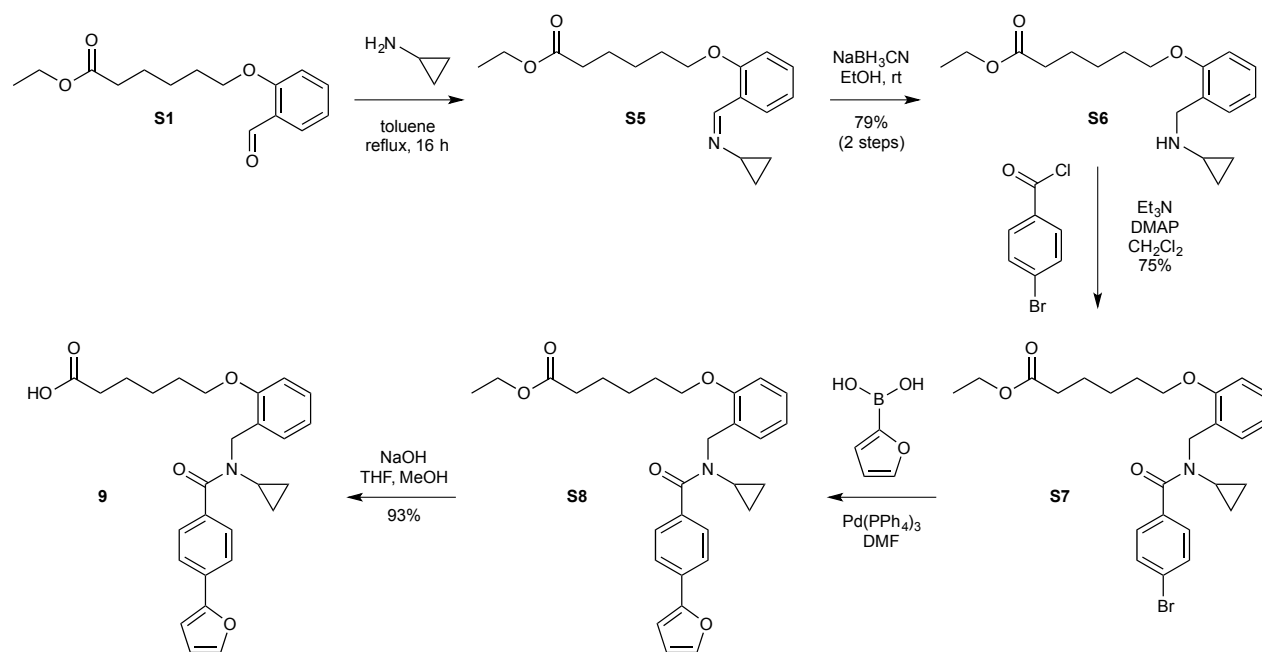
Ethyl 6-(2-((N-isopropyl-[1,1'-biphenyl]-4-carboxamido)methyl)phenoxy)hexanoate (S4). 4'-Hydroxy-1,1'-biphenyl-4-carboxylic acid (**S3**) (6.67 g, 33.67 mmol) was dissolved in CH_2Cl_2 (180 mL) in a 500 mL round bottom flask equipped with a 200 mL addition funnel. A water-cooled coil reflex condenser was placed on top of the addition funnel. Oxalyl chloride (4.81 mL, 56.1 mmol) was added at rt. DMF (0.5 mL) was added slowly causing vigorous gas release and heating. After stirring at rt for 1.5 h, the solvent was removed by distillation into the addition funnel using an oil bath at 70 °C. The resulting solid was dried under vacuum over 2 h. Crude amine **S3** (6.90 mmol, 22.44 mmol) was dissolved in CH_2Cl_2 (180 mL) and cooled to 0°C. Et_3N (18.79 mL, 134.66 mmol) and DMAP (0.27 g, 2.24 mmol) were added sequentially. The resulting acid chloride was removed from vacuum drying, dissolved in CH_2Cl_2 (100 mL), and added dropwise fashion to the amine via an addition funnel. The mixture was warmed to rt over 1 h and stirred overnight at rt. The mixture was diluted with CH_2Cl_2 (100 mL) and sequentially washed with 1 N HCl (50 mL), H_2O (2 × 50 mL), satd. $NaHCO_3$ (50 mL), and brine (50 mL). The crude product was obtained by drying over Na_2SO_4 and concentration on a rotary evaporator. Pure ester **S4** (4.06 g, 37% from **S1**) was obtained by flash chromatography eluted with a gradient of hexanes to 1:2 hexanes:EtOAc.

Ester **S4**: 1H NMR ($CDCl_3$, 500 MHz) δ 7.59 (m, 3H), 7.52 (m, 2H), 7.44 (m, 2H), 7.36 (m, 3H), 7.19 (dt, $J = 1.7, 7.8$ Hz, 1H), 6.95 (t, $J = 7.5$ Hz, 1H), 6.82 (m, 1H), 4.73 (s, 1H), 4.13 (q, $J = 7.1$ Hz, 2H), 4.01 (m, 2H), 2.34 (m, 2H), 1.84 (m, 2H), 1.72 (m, 2H), 1.61 (m, 1H), 1.26 (t, $J = 7.2$ Hz, 3H), 1.14 (m, 2H); ^{13}C NMR ($CDCl_3$, 125 MHz) δ 173.7, 155.9, 140.6, 136.6, 129.0, 127.8, 127.7, 127.2, 127.0, 120.6, 111.1, 67.8, 60.4, 34.4, 29.2, 25.9, 24.9, 21.1, 14.4; HR-ESI-MS m/z calcd. for $C_{31}H_{37}NO_4$ $[M+Na]^+$: 510.2615, found 510.2614.

6-(2-((N-isopropyl-[1,1'-biphenyl]-4-carboxamido)methyl)phenoxy)hexanoic acid (1). Ester **S4** (0.20 g, 0.41 mmol) was dissolved in THF (1.5 mL) and MeOH (1.5 mL). At rt, 3 M NaOH (1.4 mL) was added and the mixture was stirred at rt. After 7 h, TLC analysis indicated that the reaction was complete. The pH was adjusted to 4 by adding 1 M HCl in dioxanes, and the mixture was dried via rotary evaporation. Pure compound **1** (0.17 g, 91%) was obtained after purification via pTLC on a 500 μm 20 cm × 20 cm plate using a chamber loaded with 1:2 EtOAc:MeOH.

Compound **1**: 1H NMR ($CDCl_3$, 500 MHz) δ 7.65 (m, 2H), 7.60 (m, 2H), 7.54 (m, 2H), 7.46 (m, 3H), 7.38 (m, 1H), 7.28 (m, 1H), 7.18 (t, $J = 7.8$ Hz, 1H), 6.93 (t, $J = 7.5$ Hz, 1H), 6.82 (d, $J = 8.1$ Hz, 1H), 5.36 (bm, 1H), 4.71 (m, 2H), 4.52 (m, 2H), 4.21 (m, 2H), 4.00 (m, 2H), 3.83 (m, 2H), 2.25 (m, 2H), 1.82 (m, 2H), 1.64 (m, 2H), 1.53 (m, 2H), 1.25 (m, 2H), 1.10 (m, 3H); ^{13}C NMR ($CDCl_3$, 125 MHz) δ 173.7, 131.2, 129.2, 128.6, 125.6, 123.9, 120.4, 111.2, 67.8, 60.3, 34.2, 29.1, 25.7, 24.7, 14.3; HR-ESI-MS m/z calcd. for $C_{29}H_{33}NO_4$ $[M+Na]^+$: 482.2302, found 482.2302.

A.9. Preparative synthesis of 9. Compound **9** was prepared in 5 steps in 28% overall yield from intermediate **S1**. Scheme S3 and the following sections describe the methods, materials, and spectral data analyses for intermediates and the final product **9**.



Scheme S3. Synthesis of compound **9**. Preparation of **9** required three chromatographic purifications as the crude **S5** and **S6** could be used without additional purification.

Ethyl 6-(2-((cyclopropylamino)methyl)phenoxy)hexanoate (S6). Aldehyde **S1** (4.5 g, 17.0 mmol) and cyclopropylamine (3.5 mL, 51.1 mmol) were dissolved in THF (100 mL). Powdered and dried 4 Å molecular sieves (5 g) were added. After stirring overnight, the reaction mixture was filtered through a pad of dry SiO_2 (200 g), washed with EtOAc, and dried by rotary evaporation to yield imine **S5**, which was used immediately without further purification.

Crude imine **S5** (5.16 g, 17.0 mmol) was dissolved in EtOH (100 mL) and cooled to 0°C. NaBH_3CN (3.21 g, 51.1 mmol) was added in 5 portions over 20 min. The mixture was then stirred overnight at rt. TLC analysis indicated ~85% completion. An additional aliquot of NaBH_3CN (0.8 g, 12.8 mmol) was then added, and the mixture was again stirred overnight. The reaction was terminated by the addition of 1 N NaOH (100 mL), extracted with EtOAc (3 × 200 mL), and washed with brine (100 mL). The crude product was obtained by drying over Na_2SO_4 and concentration on a rotary evaporator. The resulting amine **S6** (4.52 g, 87%) was sufficiently pure (~95%) for the next step. Alternatively, pure material was obtained by flash chromatography eluted with a gradient of hexanes to 1:2 hexanes:EtOAc.

Amine S6: ^1H NMR (CDCl_3 , 500 MHz) δ 7.28 (dd, $J = 1.8, 7.4$ Hz, 1H), 7.23 (td, $J = 1.8, 8.0$ Hz, 1H), 6.90 (dt, $J = 1.0, 7.4$ Hz, 1H), 6.85 (d, $J = 8.2$ Hz, 1H), 4.13 (q, $J = 7.1$ Hz, 2H), 4.00 (t, $J = 6.4$ Hz, 2H), 3.89 (s, 1H), 2.34 (t, $J = 7.5$ Hz, 1H), 2.13 (tt, $J = 3.7, 6.9$ Hz, 2H), 1.84 (td, $J = 6.6, 14.1$ Hz, 2H), 1.71 (p, $J = 7.5$ Hz, 2H), 1.53 (m, 2H), 1.25 (t, $J = 7.1$ Hz, 3H), 0.55 (m, 2H); ^{13}C NMR (CDCl_3 , 125 MHz) δ 173.7, 157.1, 130.4, 128.6, 120.3, 111.1, 67.5, 60.4, 49.2, 34.3, 29.6, 29.1, 25.8, 24.7, 14.2, 6.0; HR-ESI-MS m/z calcd. for $\text{C}_{18}\text{H}_{27}\text{NO}_3$ $[\text{M}+\text{H}]^+$: 306.2064, found 306.2064.

Ethyl 6-(2-((4-bromo-N-cyclopropylbenzamido)methyl)phenoxy)hexanoate (S7). Amine **S6** (4.12 g, 13.40 mmol) was dissolved in CH_2Cl_2 (120 mL), and Et_3N (11.2 mL, 80.4 mmol) along with DMAP (0.16 g, 1.34 mmol) were added sequentially. The mixture was cooled to 0°C and 4-bromobenzoylchloride (5.29 g, 24.12 mmol) was added in CH_2Cl_2 (40 mL). After warming to rt and stirring overnight, CH_2Cl_2 (100 mL) was added, the mixture was washed sequentially with 1N HCl (50 mL), water (2×50 mL), satd. NaHCO_3 (50 mL), and brine (50 mL). The crude product was obtained by drying over Na_2SO_4 and concentration on a rotary evaporator. Pure amide **S7** (4.92 g, 75%) was obtained by flash chromatography eluted with a gradient of hexanes to 1:2 hexanes:EtOAc.

Amide S7: ^1H NMR (CDCl_3 , 500 MHz) δ 7.52 (d, $J = 8.1$ Hz, 2H), 7.43 (d, $J = 8.2$ Hz, 2H), 7.27 (m, 2H), 6.94 (t, $J = 7.4$ Hz, 1H), 6.88 (d, $J = 8.2$, 1H), 4.77 (bs, 1H), 4.13 (q, $J = 7.1$ Hz, 2H), 4.00 (t, $J = 6.6$ Hz, 2H), 2.59 (td, $J = 3.2, 6.7$ Hz, 1H), 2.29 (t, $J = 7.5$ Hz, 2H), 1.79 (p, $J = 6.9$ Hz, 2H), 1.67 (p, $J = 1.67$, 2H), 1.50 (m, 2H), 1.26 (t, $J = 7.2$ Hz, 3H), 0.51 (m, 4H); ^{13}C NMR (CDCl_3 , 125 MHz) δ 173.6, 131.2, 129.2, 128.6, 125.5, 123.9, 120.3, 111.1, 67.8, 60.3, 46.1, 34.2, 31.9, 29.1, 25.7, 24.7, 14.3, 10.0; HR-ESI-MS m/z calcd. for $\text{C}_{25}\text{H}_{30}\text{BrNO}_4$ $[\text{M}+\text{Na}]^+$: 510.1250, found 510.1249.

Ethyl 6-(2-((N-cyclopropyl-4-(furan-2-yl)benzamido)methyl)phenoxy)hexanoate (S8). Amide **S7** (2.05 g, 4.20 mmol) and 2-furanylboronic acid (0.71 g, 6.31 mmol) were dissolved in DMF (10 mL). The solution was degassed and charged with Ar. Fresh $\text{Pd}(\text{PPh}_3)_4$ (0.49 g, 0.42 mmol) was added, the mixture was immediately degassed and charged with Ar, and heated to 60°C . After stirring overnight, EtOAc (200 mL) was added, the mixture was washed sequentially with satd. NaHCO_3 (50 mL) and brine (50 mL). The crude product was obtained by drying over Na_2SO_4 and concentration on a rotary evaporator. Pure ester **S8** (1.38 g, 69%) was obtained by flash chromatography eluted with a gradient of hexanes to 1:1 hexanes:EtOAc.

Ester S8: ^1H NMR (CDCl_3 , 500 MHz) δ 7.52 (d, $J = 8.1$ Hz, 2H), 7.43 (ds, $J = 8.2$ Hz, 2H), 7.27 (m, 2H), 6.94 (t, $J = 7.4$ Hz, 1H), 6.88 (d, $J = 8.2$, 1H), 4.77 (bs, 1H), 4.13 (q, $J = 7.1$ Hz, 2H), 4.00 (t, $J = 6.6$ Hz, 2H), 2.59 (td, $J = 3.2, 6.7$ Hz, 1H), 2.29 (t, $J = 7.5$ Hz, 2H), 1.79 (p, $J = 6.9$ Hz, 2H), 1.67 (p, $J = 1.67$, 2H), 1.50 (m, 2H), 1.26 (t, $J = 7.2$ Hz, 3H), 0.51 (m, 4H); ^{13}C NMR (CDCl_3 ,

125 MHz) δ 173.8, 153.4, 142.6, 132.0, 128.9, 128.5, 128.2, 128.1, 125.9, 123.3, 120.5, 120.4, 111.9, 111.2, 106.1, 67.8, 60.3, 34.3, 29.1, 25.8, 24.8, 14.4; HR-ESI-MS m/z calcd. for $C_{29}H_{33}NO_5$ $[M+Na]^+$: 498.2251, found 498.2251.

6-(2-((N-Cyclopropyl-4-(furan-2-yl)benzamido)methyl)phenoxy)hexanoic acid (9). Ester **S7** (0.17 g, 0.31 mmol) was dissolved in THF (1.5 mL) and MeOH (1.5 mL). At rt, 3 M NaOH (1.4 mL) was added and the mixture was stirred at rt. After 7 h, TLC analysis indicated that the reaction was complete. The pH was adjusted to 4 by adding 1 M HCl in dioxanes and the mixture was dried via rotary evaporation. Pure compound **9** (0.13 g, 93%) was obtained after purification via pTLC on a 500 μ m 20 cm \times 20 cm plate using a chamber loaded with 1:2 EtOAc:MeOH.

Compound 9: 1H NMR ($CDCl_3$, 500 MHz) δ 7.68 (d, J = 8.1 Hz, 2H), 7.58 (m, J = 7.6 Hz, 1H), 7.49 (d, J = 1.8 Hz, 1H), 7.30 (m, 1H), 7.26 (m, 1H), 6.95 (t, J = 7.4 Hz, 1H), 6.88 (d, J = 8.3 Hz, 1H), 6.72 (d, J = 3.4 Hz, 1H), 6.49 (dd, J = 1.7, 3.4 Hz, 1H), 4.78 (m, 1H), 4.00 (dt, J = 3.5, 6.9 Hz, 1H), 2.31 (t, J = 7.4 Hz, 2H), 1.78 (p, J = 6.6 Hz, 1H), 1.66 (p, J = 7.5 Hz, 1H), 1.50 (m, 2H), 0.52 (m, 4H); ^{13}C NMR ($CDCl_3$, 125 MHz) δ 178.6, 153.3, 142.7, 132.3, 132.0, 128.6, 128.2, 125.7, 120.4, 112.0, 111.1, 106.2, 67.8, 34.1, 29.0, 25.7, 24.5, 10.3; HR-ESI-MS m/z calcd. for $C_{27}H_{29}NO_5$ $[M+Na]^+$: 470.1938, found 470.1941.

Supporting Information References

- Otwinowski Z, et al. (1997) Processing of X-ray diffraction data collected in oscillation mode. *Meth Enzymol* 276:307-326.
- Evans PR, Murshudov GN (2013) How good are my data and what is the resolution? *Acta Crystallogr D Biol Crystallogr* 69(7):1204-1214.
- Collaborative Computational Project, Number 4. (1994) The CCP4 suite: programs for protein crystallography. *Acta Crystallogr D Biol Crystallogr* 50(5):760-763.
- Emsley P, Lohkamp B, Scott WG, Cowtan K (2010) Features and development of Coot. *Acta Crystallogr D Biol Crystallogr* 66(4): 486-501.
- Adams PD, et al. (2010) PHENIX: a comprehensive Python-based system for macromolecular structure solution. *Acta Crystallogr D Biol Crystallogr* 66(2): 213-221.
- Mitachi, K, et al. (2012) Synthesis and structure-activity relationship of disubstituted benzamides as a novel class of antimalarial agents. *Bioorg. Med. Chem. Lett.* 22(14): 4536-4539.
- Laskowski RA, Swindells MB (2011) LigPlot+: multiple ligand-protein interaction diagrams for drug discovery. *J Chem Inf Model* 51(10):2778-2786.

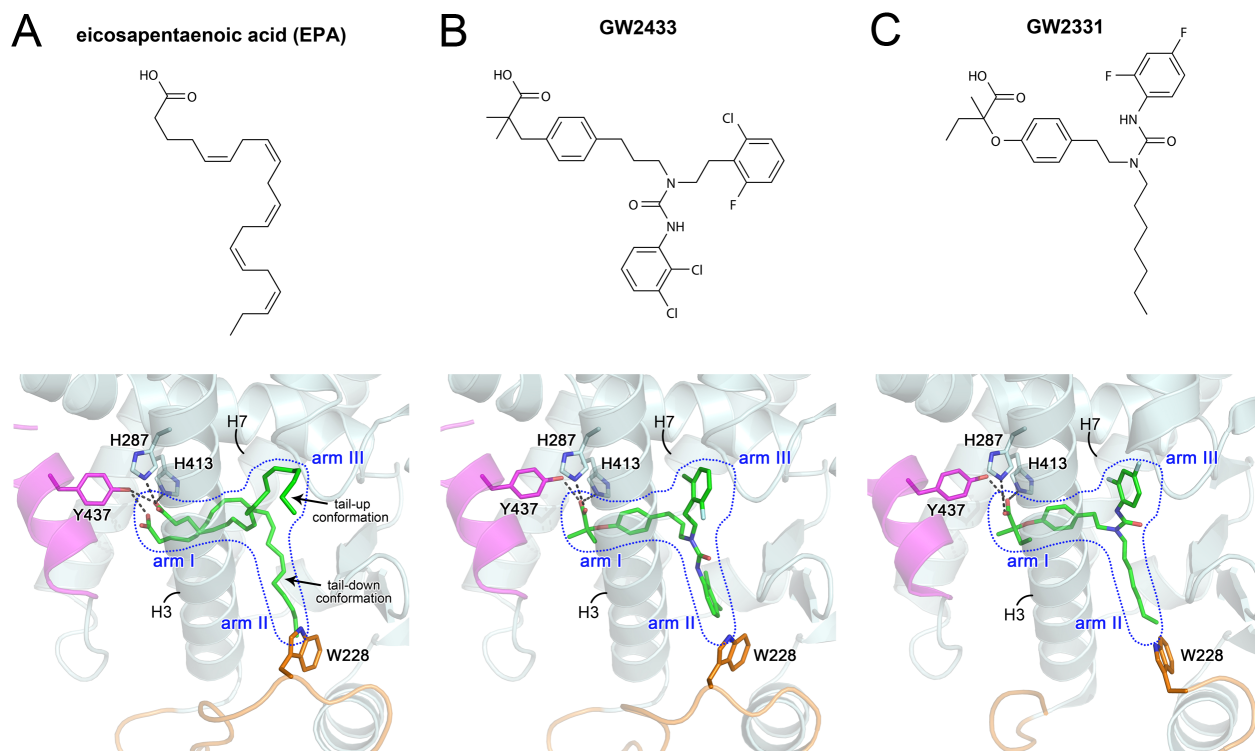


Fig. S1. The reported structures of ligand-bound hPPAR δ -LBDs. The ligand-binding site of (A) eicosapentaenoic acid (EPA) (PDB ID:3GWX) (27), (B) GW2433 (PDB ID:1GWX) (27) and (C) GW2331 (PDB ID:1Y0S) (28). The Y-shaped ligand-binding pockets of hPPAR δ -LBDs are illustrated by blue dashed lines. The three extended arms (arm I, II and III) of the Y-shaped pockets are labeled. Hydrogen bonds between the ligands and residues Y437, H287 and H413 are shown as black dashed lines. The activation factor-2s (AF-2) and the H2'-H3 loops of hPPAR δ -LBDs are highlighted in purple and orange, respectively.

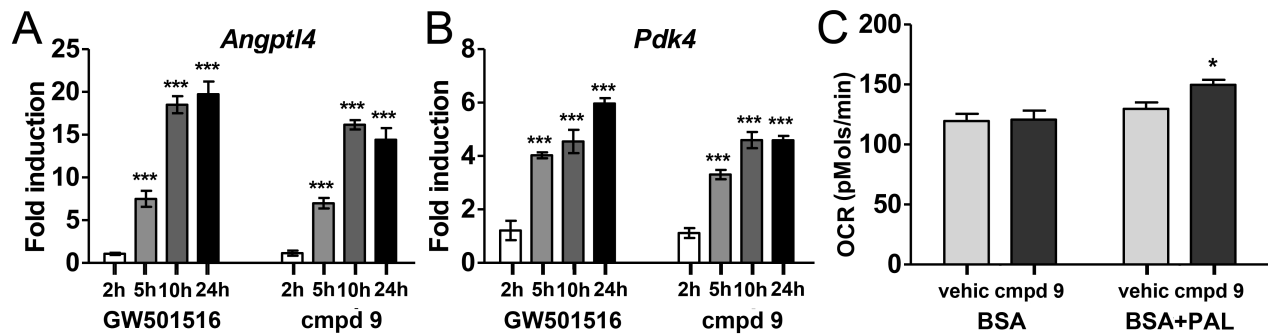


Fig. S2. Cell-based PPAR δ agonist activity. Compound 9 (cmpd 9) and GW501516 induced similar time-dependent induction on PPAR δ target genes in differentiated C2C12 myotubes including *Angptl4* (A) and *Pdk4* (B). Gene expression levels were normalized to DMSO-treated controls and presented as fold inductions. (C) 15 hr treatment of differentiated myotubes with compound 9 significantly increased palmitate-fueled OCRs (BSA+PAL) while the glucose-fueled OCRs were not affected (BSA). Vehicle (vehic) used was DMSO.

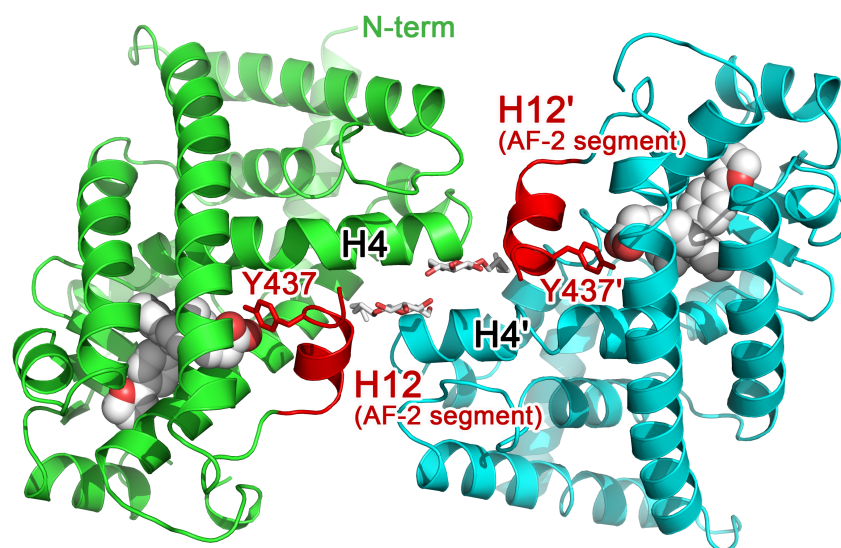


Fig. S3. The two polypeptide chains per asymmetry unit of the **9**•hPPAR δ -LBD complex structure. The polypeptide chains related by a non-crystallographic two-fold rotation axis are colored green and cyan, respectively, with the AF-2 helical segments colored red in both cases. Ligands (compound **9**) are shown in van der Waals spheres with carbon light gray, oxygen red and nitrogen blue. Labels belonging to the cyan chain are highlighted with primes. The two heptyl- β -D-glucopyranoside molecules straddle the non-crystallographic two-fold axis and are shown as color-coded sticks. The side chains of Y437 are shown as red sticks.

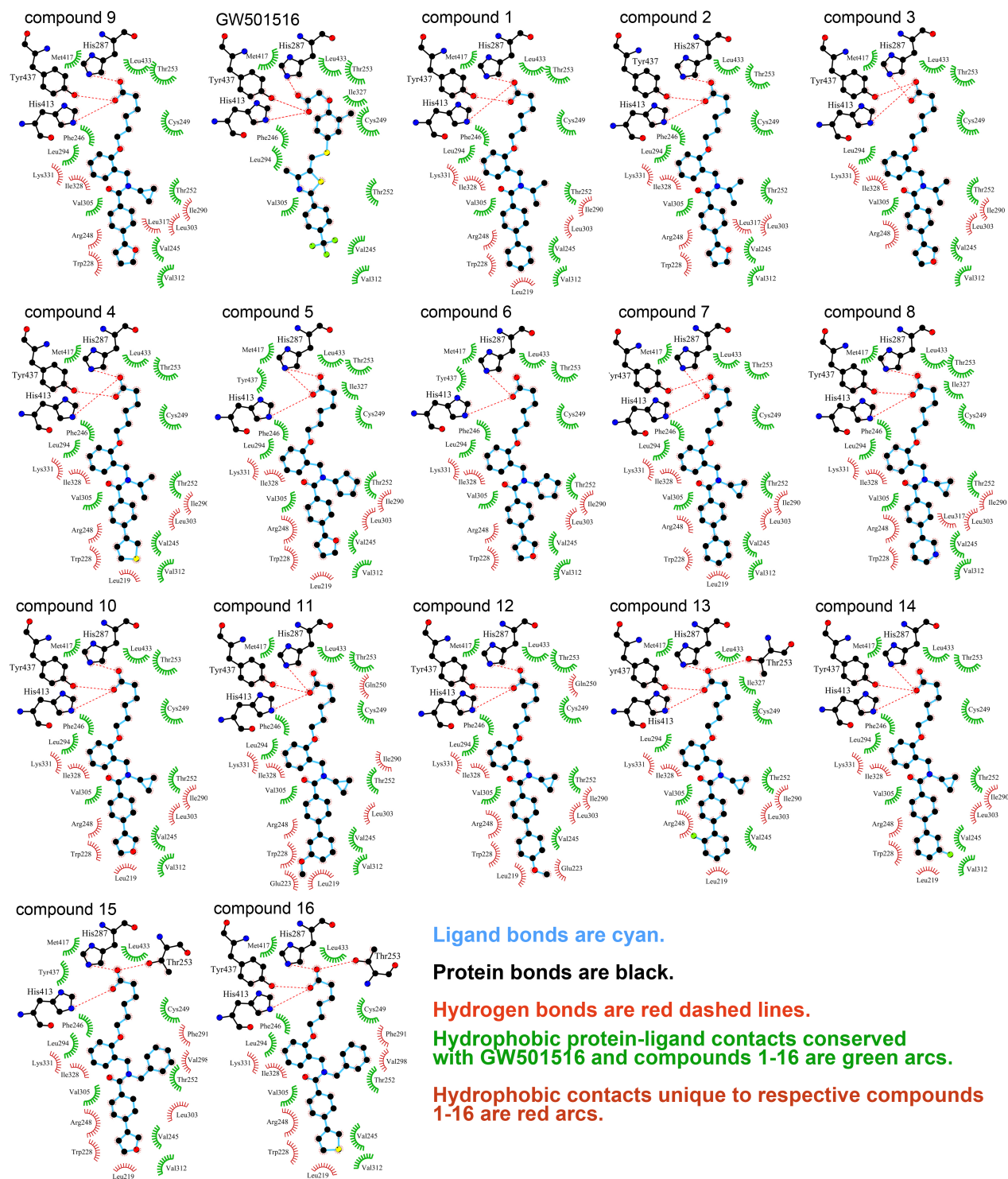


Fig. S4. Interatomic interactions of ligands with hPPAR δ -LBDs. Conserved hydrogen bonds between the ligands' carboxyl groups and H287, H413 and Y437 in the arm I ligand-binding pockets are illustrated by red dashed lines. All plots were generated using LigPlot+ (60).

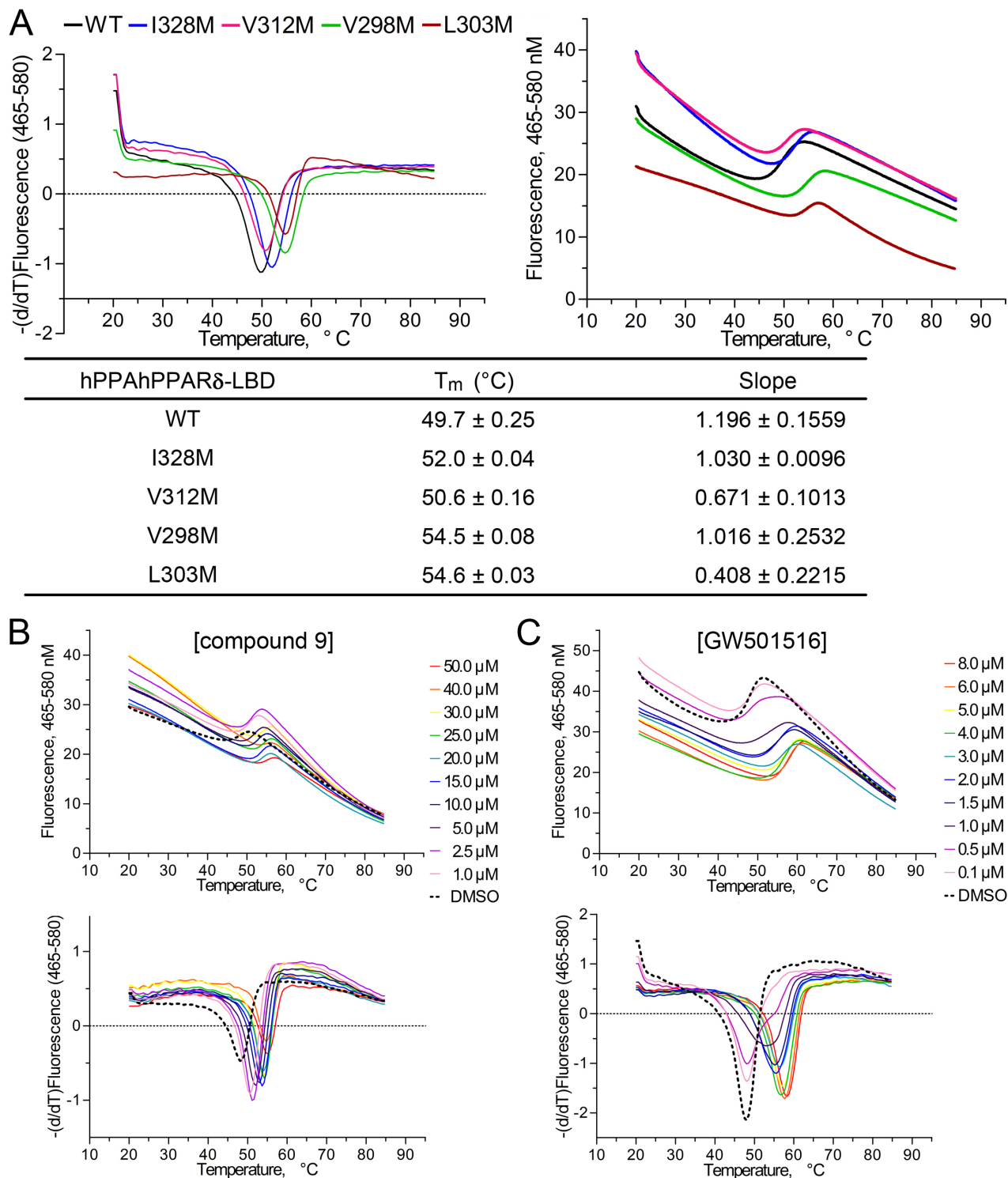


Fig. S5. Thermostability analyses. (A) The protein melting curves (right panels) and their reciprocal derivative curves (left panels) of the wild-type and mutated hPPAR δ -LBDs. For each reaction, 0.6 μ g protein was mixed with 1 μ L of 20 \times SYPRO Orange dye. The melting temperatures (T_m s) and slopes of each curve were determined by using LightCycler 480 Software, Version 1.5. (B and C). Thermal-shift binding assays of wild-type hPPAR δ -LBDs

interacting with compound **9** (CBPL-89) and GW501516, respectively. For (*B* and *C*), the melting curves are shown in the upper panels and their reciprocal derivative curves are illustrated in the lower panels. For each thermal-shift binding assay, 0.6 μg hPPAR δ -LBD was mixed with 1 μL of 20 \times SYPRO Orange dye and 1 μl of serially diluted ligands in 100% (v/v) DMSO. The final concentration of DMSO was held constant at 10% (v/v). The plots are fit and illustrated using GraphPad Prism v5.04.

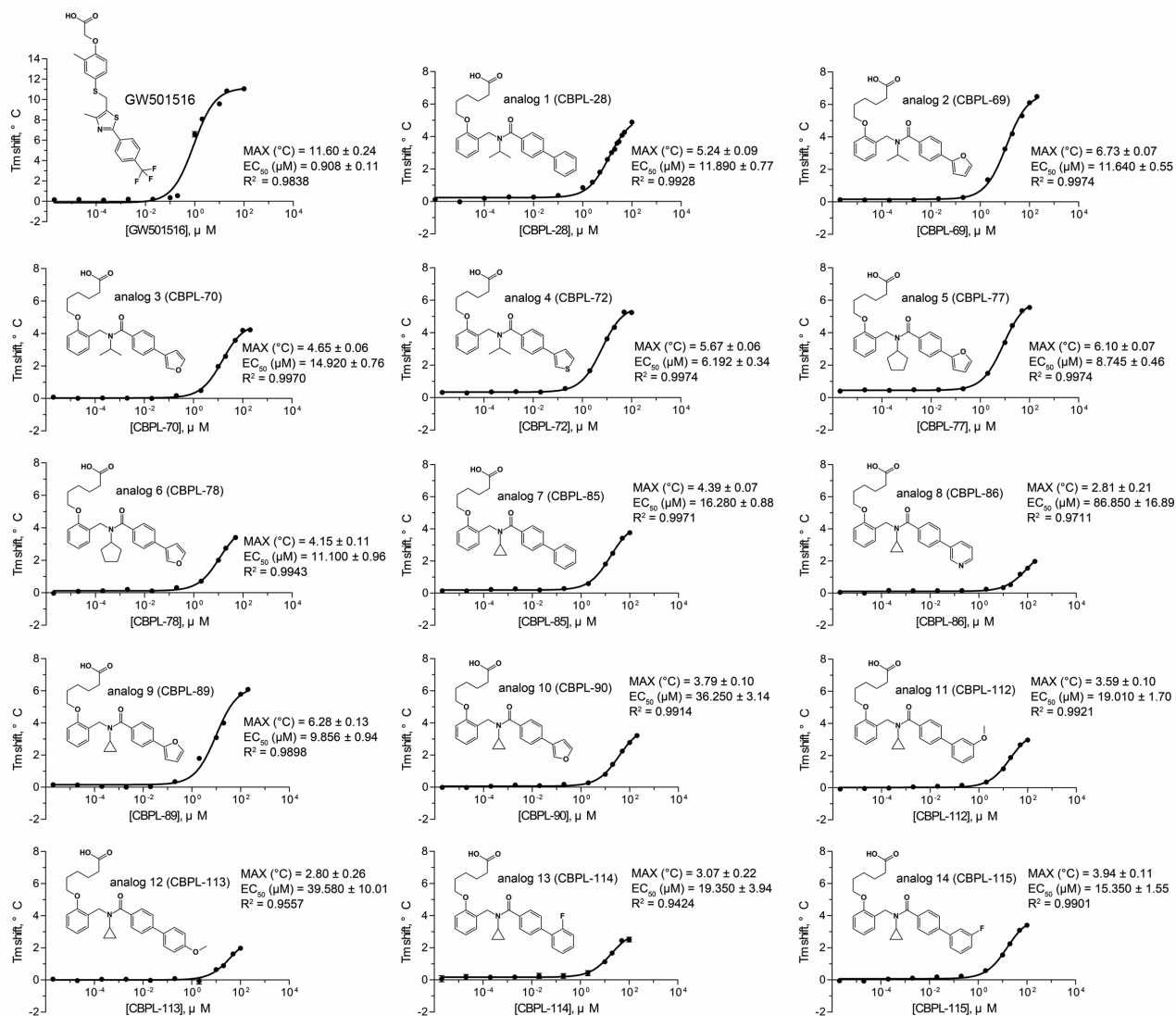


Fig. S6. Thermostabilization effects of GW501516 and compounds **1-14** for wild-type hPPAR δ -LBDs. For each thermal-shift binding assay, 0.6 μ g hPPAR δ -LBD was mixed with 1 μ L of 20 \times SYPRO Orange dye and 1 μ L of serially diluted ligands in 100% (v/v) DMSO. The final concentration of DMSO was held constant at 10% (v/v). The results were fitted using three-parameter dose-response curve analyses in GraphPad Prism v5.04. Data points are shown as mean \pm SE, where $n \geq 3$. The estimated maximum T_m shifts, EC_{50} and R^2 values are listed beside each plot.

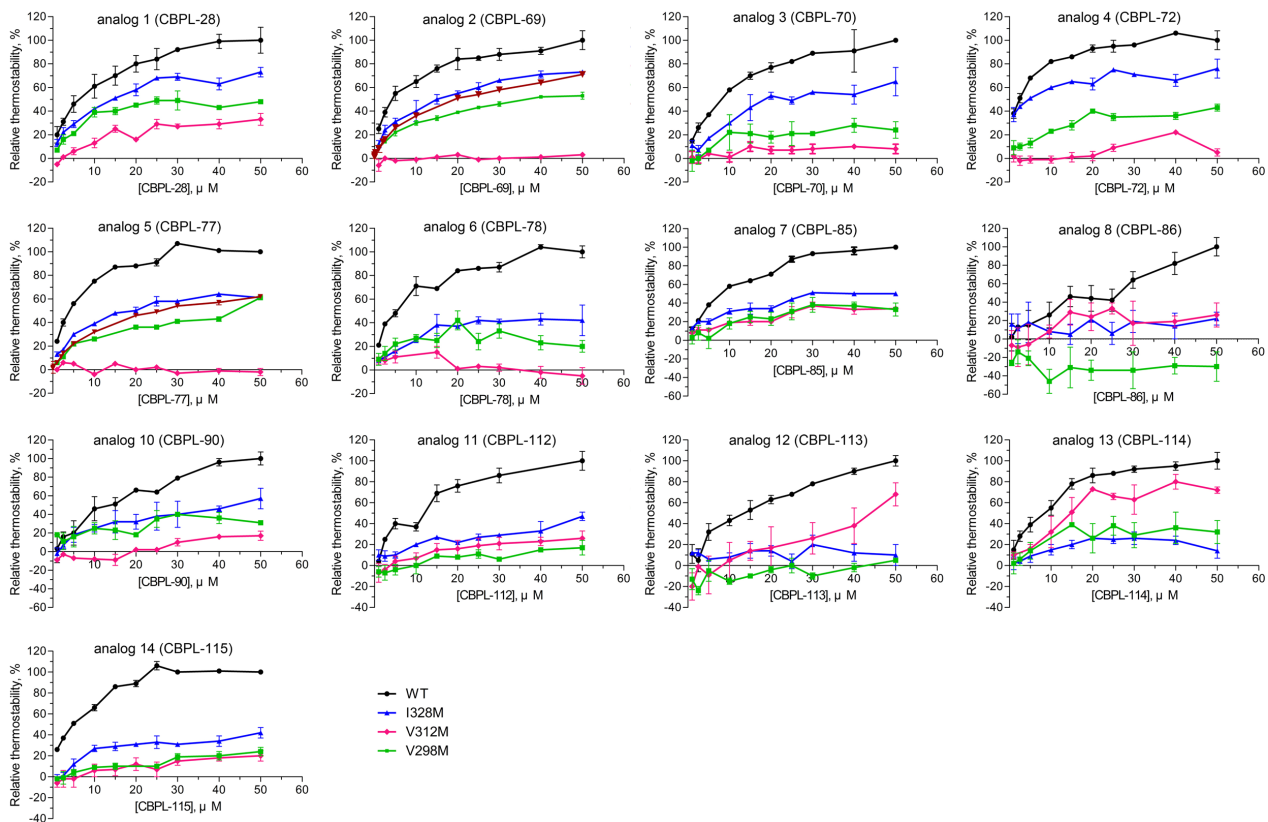


Fig. S7. Thermal-shift binding assays of wild-type and mutated hPPAR δ -LBDs interacting with GW501516 and compounds **1-8** and **10-14**. Data points are shown as mean \pm SE, where n = 3. The plots are drawn using GraphPad Prism v5.04.

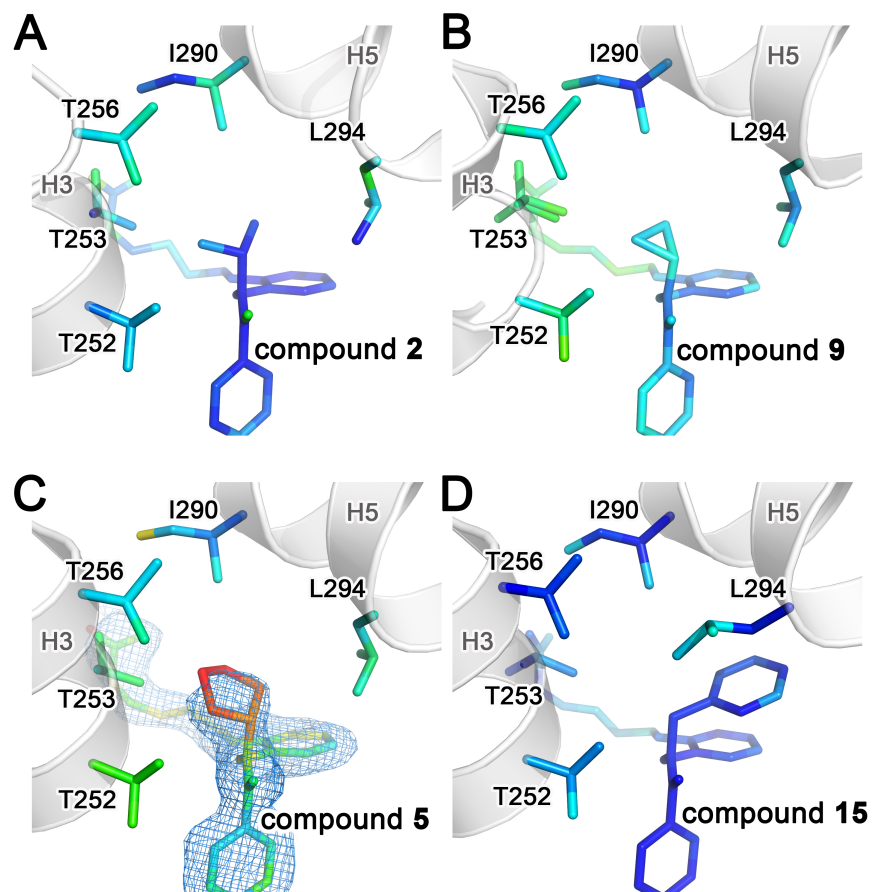


Fig. S8. Four chemotypes of R₁ of newly reported compounds. The ligand-binding site of the (A) **2**•hPPAR δ -LBD, (B) **9**•hPPAR δ -LBD, (C) **5**•hPPAR δ -LBD, and (D) **15**•hPPAR δ -LBD structures highlighting R₁ functional moieties, isopropyl in (A), cyclopropyl in (B), cyclopentyl in (C), and benzyl in (D). For each panel, ligand and selected side chains are shown as color-coded sticks according to variation in atomic displacement parameters (B-factors) (blue low; red high). For (C), the weighted electron density map ($2mF_o - DF_c$) contoured at $\sigma = 1.0$ of the bound ligand is shown as a blue mesh.

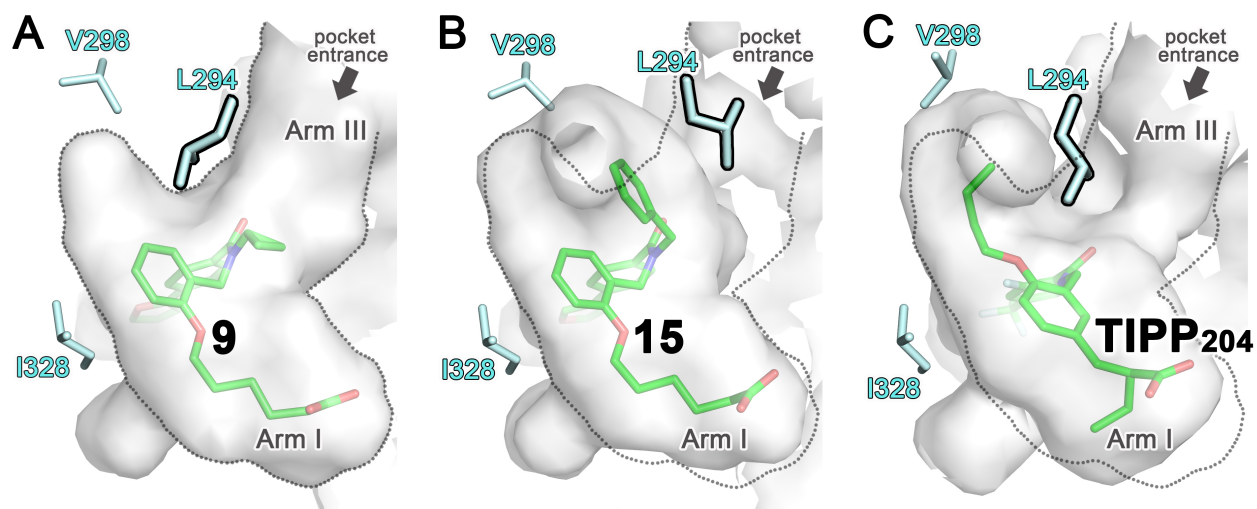


Fig. S9. Alternative landscapes of PPAR δ ligand-binding pockets gated by the side chain conformations of L294. Surface representation of the ligand-binding pockets of (A) **9**•hPPAR δ -LBD, (B) **15**•hPPAR δ -LBD, and (C) TIPP204•hPPAR δ -LBD (PDB ID: 2ZNP) (39). The three models were aligned by matching secondary structures. For each panel, the overall shape of the ligand-binding pocket in the **9**•hPPAR δ -LBD structure is illustrated by gray dotted lines to highlight the differences in accessible volume of the three complex structures. Ligands are shown as color-coded sticks with carbon green and oxygen red. Selected side chains are shown as light blue sticks. The side chains of L294 are emphasized with thick black lines.

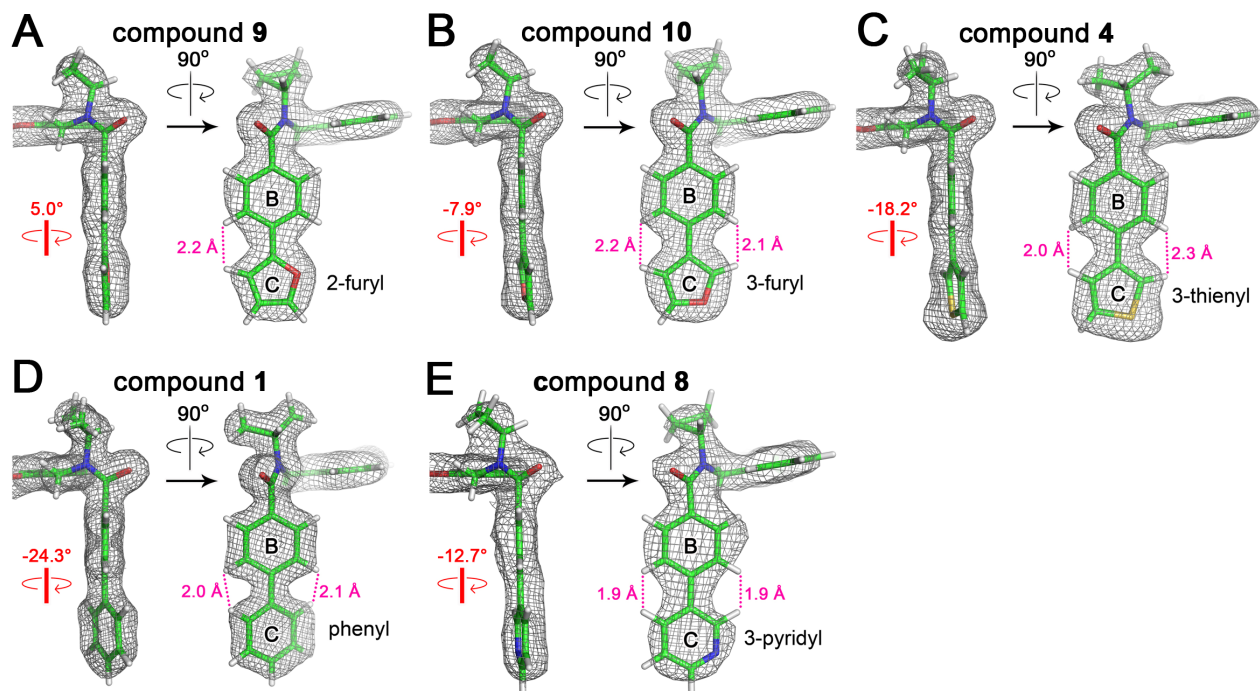


Fig. S10. Torsion angles defining the orientations of B rings relative to C rings of the bound ligands in refined hPPAR δ -LBD structures. Orthogonal views of the hPPAR δ -LBDs bound to (A) **9**, (B) **10**, (C) **4**, (D) **1** and (E) **8**. For all panels, ligands are shown as color-coded sticks with carbon green, oxygen red, nitrogen blue, and sulfur yellow. Weighted electron density maps are shown as gray meshes ($2mF_o-DF_c$) contoured at $\sigma = 1.0$. The average torsion angles between B and C rings of the ligands observed in each asymmetric unit are labeled in red (for further details see Table S3). Pink dashed lines and distances in Å indicate close contacts between the ortho-hydrogens that partially orient ring B relative to ring C.

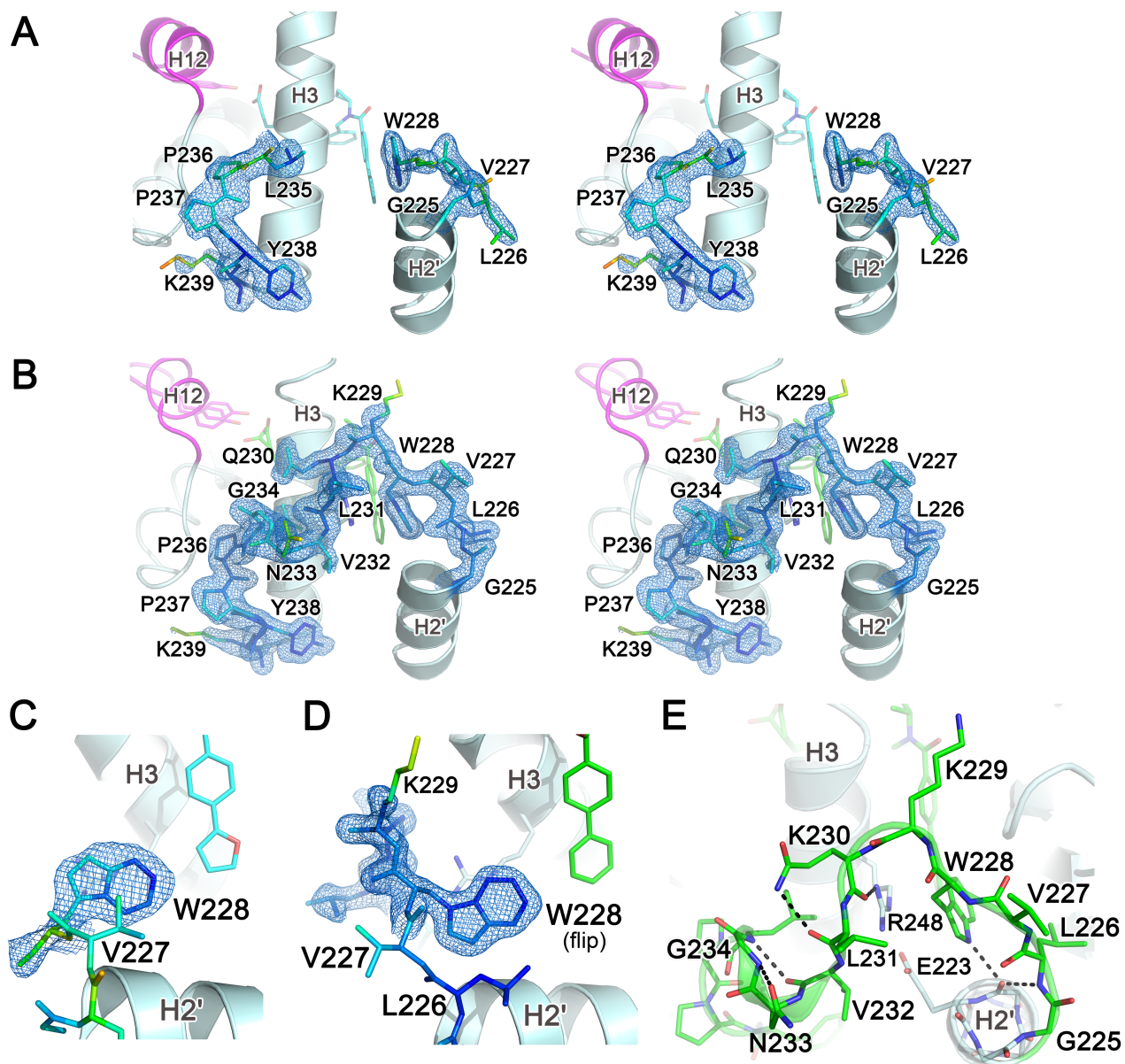


Fig. S11. Ligand-dependent conformational switching of the H2'-H3 loops for hPPAR δ -LBDs. (*A* and *B*) Stereo views of the H2'-H3 loop region in the 9•hPPAR δ -LBD and 1•hPPAR δ -LBD structures, respectively. (*C* and *D*) Close-up views of the H2'-H3 loop region in the 9•hPPAR δ -LBD and 1•hPPAR δ -LBD structures, respectively. For panels *A-D*, the weighted $2mF_o - DF_c$ electron density maps are contoured at 1.0σ for the loop regions and shown as blue meshes. Residues G225 to K239 for both hPPAR δ -LBD ligand complexes are shown as color-coded sticks according to atomic displacement parameters (B-factors) of refined atoms (red: high B-factors; blue: low B-factors). Compounds 9 and 1 are shown as color-coded sticks with carbons cyan and green, respectively. The AF-2 helical segments harboring Y437 are colored magenta. (*E*) The ordered loop conformation of the 1•hPPAR δ -LBD structure. The H2'-H3 loop is colored green. Stabilizing hydrogen bonds are illustrated by black dashed lines.

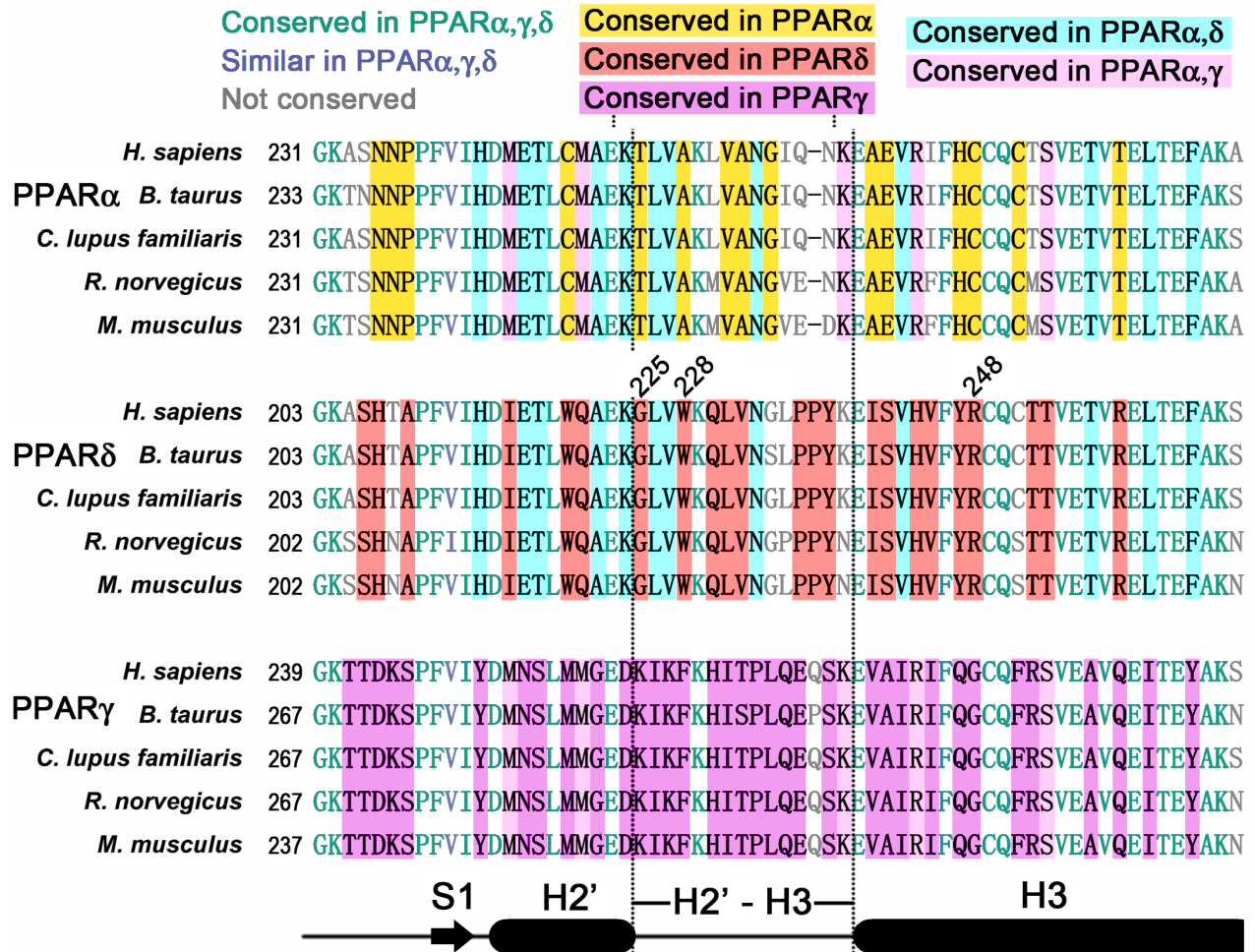


Fig. S12. Amino acids sequence alignments of the H2'-H3 regions of phylogenetically diverse PPARs. For clarity, isoform 1 for human PPAR δ and isoform 1 for human PPAR γ , were used for alignment and numbered accordingly. Human (*Homo sapien*); Bovine (*Bos taurus*); Domesticated dog (*Canis lupus familiaris*); Rat (*Rattus norvegicus*); and Mouse (*Mus musculus*).

Table S1. Data collection and refinement statistics.

Protein	hPPAR δ -LBD (residues 170-441)								
Ligand	1 (CBPL-28)	2 (CBPL-69)	3 (CBPL-70)	4 (CBPL-72)	5 (CBPL-77)	6 (CBPL-78)	7 (CBPL-85)	8 (CBPL-86)	9 (CBPL-89)
PDBid	5U3Q	5U3R	5U3S	5U3T	5U3U	5U3V	5U3W	5U3X	5U3Y
Space group	<i>P 1 2₁ 1</i>								
Unit cell dimensions <i>a, b, c</i> (Å), β (°)	39.46, 94.35, 96.73, 98.36	39.6, 94.58, 96.22, 97.88	39.55, 94.19, 96.32, 98.08	39.64, 94.69, 96.43, 97.99	39.6, 94.55, 96.57, 97.91	39.61, 95.05, 96.32, 97.87	39.56, 94.81, 96.61, 98.27	39.1, 92.94, 96.16, 98.03	39.44, 94.94, 96.01, 97.53
Data collection									
Resolution range (Å)	95.70-1.5 (1.53-1.50)	94.58-1.95 (2.00-1.95)	67.01-1.85 (1.89-1.85)	94.69-1.70 (1.73-1.70)	47.83-1.85 (1.89-1.85)	95.05-1.84 (1.87-1.84)	94.81-1.55 (1.58-1.55)	92.94-1.80 (1.83-1.80)	95.18-1.85 (1.89-1.85)
Observed reflections	439212 (3601)	154965 (11067)	142438 (8932)	187933 (2436)	118926 (7288)	208952 (3837)	309928 (2528)	202787 (3295)	183377 (3883)
Unique reflections	92879 (1583)	51078 (3608)	59151 (3695)	72951 (2021)	48868 (3185)	59681 (2150)	85744 (2131)	57201 (2208)	54673 (2470)
Multiplicity	4.7 (2.3)	3.0 (3.1)	2.4 (2.4)	2.6 (1.2)	2.4 (2.3)	3.5 (1.8)	3.6 (1.2)	3.5 (1.5)	3.4 (1.6)
Completeness (%)	83 (28.7)	99.7 (99.9)	99.2 (99.5)	94.2 (48.9)	81.6 (86.1)	97.4 (67.8)	84.0 (42.1)	90.8 (70.8)	91.5 (70.3)
Mean I/sigma(I)	11.6 (0.8)	7.5 (1.0)	10.6 (1.1)	25.3 (4.3)	6.1 (0.7)	9.2 (0.8)	5.2 (0.5)	4.6 (0.5)	6.9 (0.7)
CC(1/2)	0.998 (0.610)	0.994(0.474)	0.994(0.424)	0.996 (0.626)	0.976 (0.437)	0.996 (0.625)	0.988 (0.403)	0.984 (0.509)	0.986 (0.395)
Data refinement									
Wilson B-factor	18.15	25.04	24.37	22.41	25.87	24.81	22.48	27.42	23.63
R-work/ R-free	0.1591/0.1893	0.1879/0.2326	0.1909/0.2469	0.1823/0.2205	0.2109/0.2608	0.2003/0.2445	0.1992/0.2463	0.2172/0.2478	0.2033/0.2445
RMSD (bonds)	0.010	0.014	0.012	0.013	0.007	0.010	0.011	0.009	0.002
RMSD (angles)	1.05	1.30	1.14	1.34	1.03	1.05	1.28	0.97	0.54
Ramachandran favored/allowed/outliers (%)	98/1.5/0	96/3.5/0.37	98/2/0	99/1.4/0	97/2.4/0.2	97/2.9/0.18	98/1.7/0	97/2.5/0	98/2.1/0
Clashscore	1.89	7.25	2.54	2.69	9.88	2.30	1.10	8.36	0.45
Average B-factor	27.77	33.90	38.91	33.59	35.78	37.67	36.76	39.57	34.95

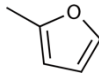
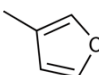
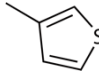
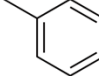
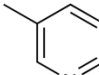
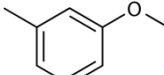
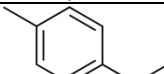
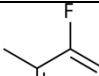
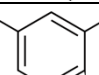
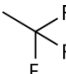
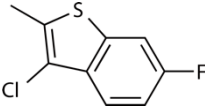
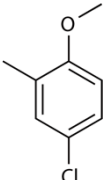
Statistics for the highest-resolution shell are shown in parentheses.

Table S2. Data collection and refinement statistics.

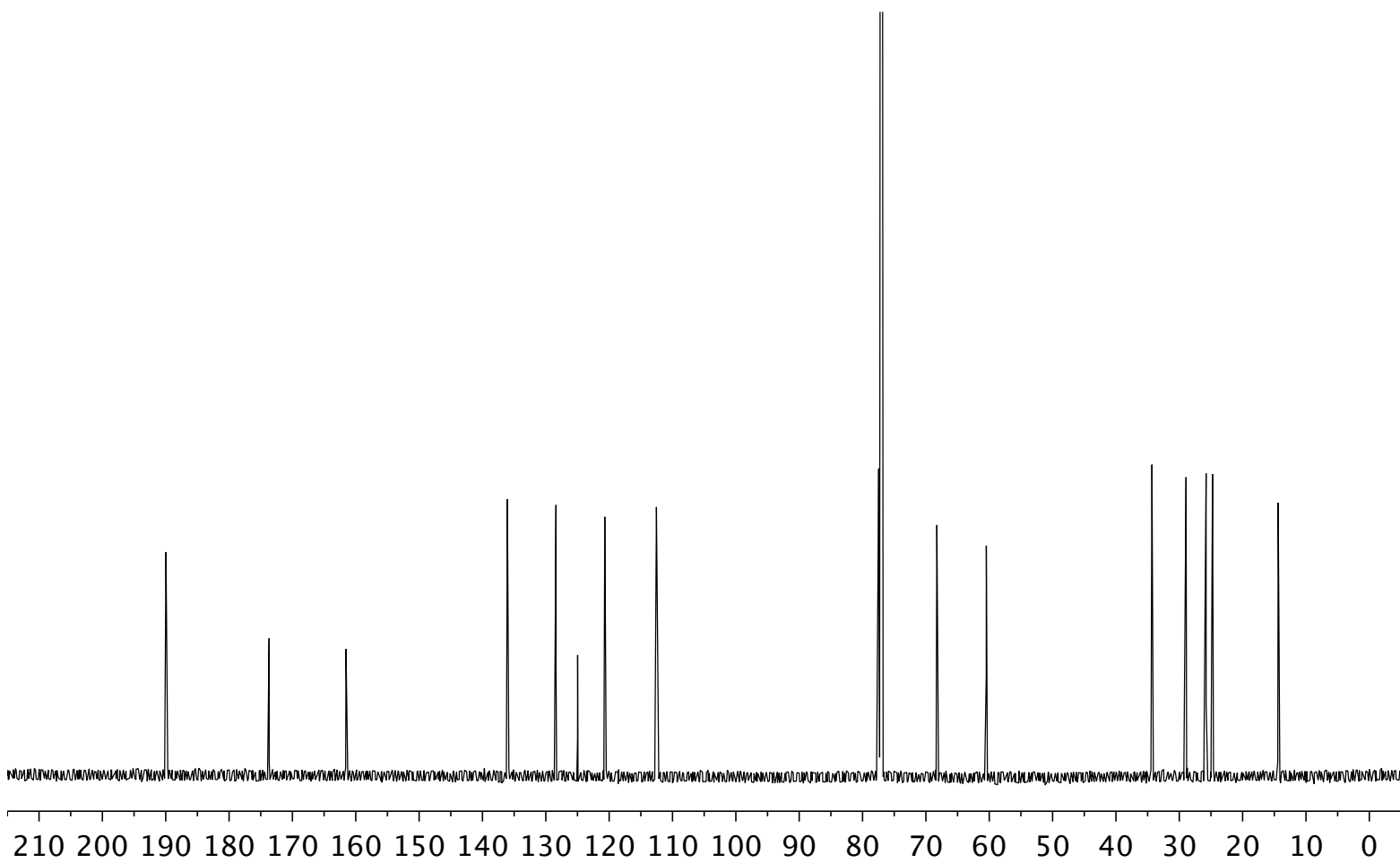
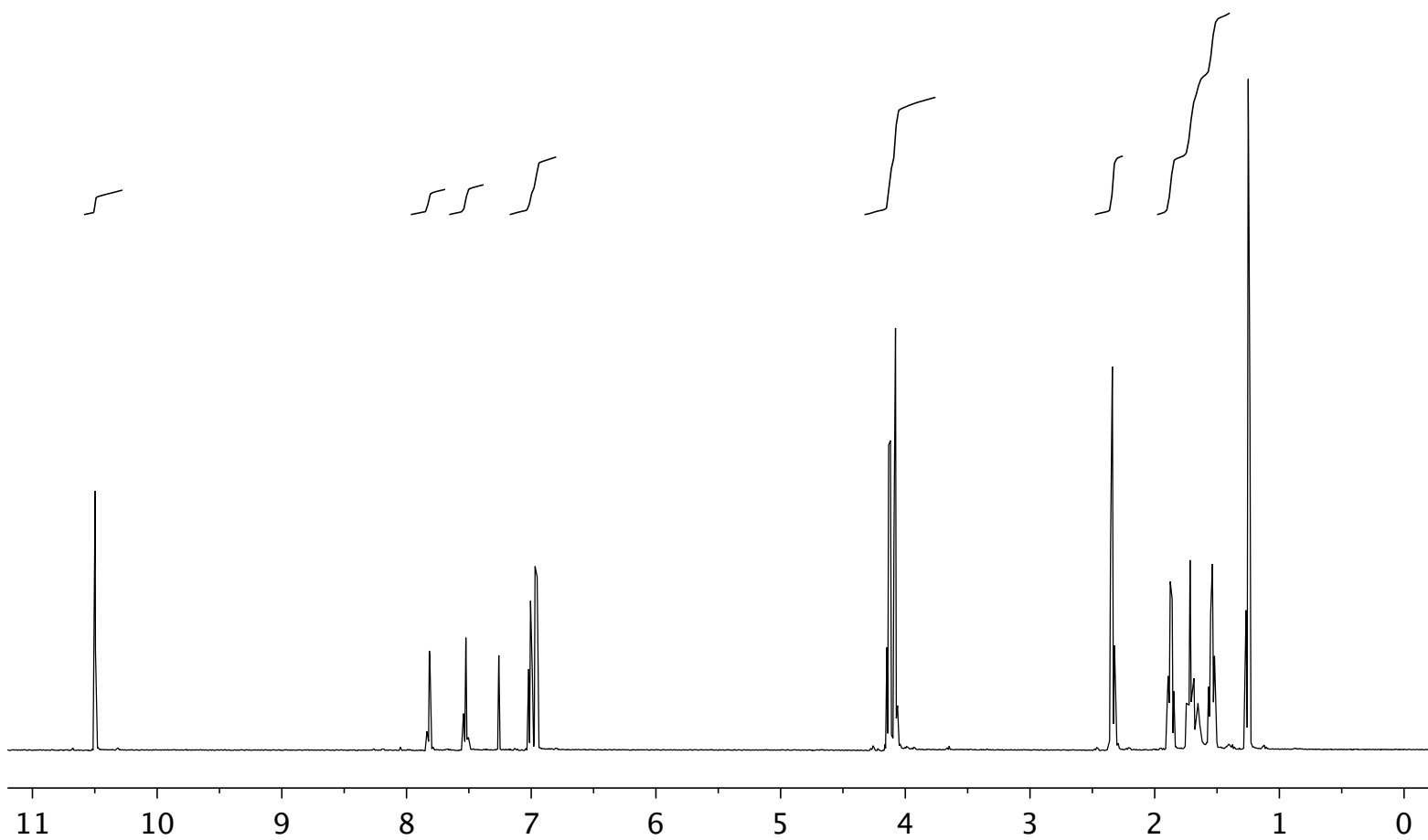
Protein	hPPAR δ -LBD (residues 170-441)							
Ligand	10 (CBPL-90)	15 (CBPL-104)	16 (CBPL-106)	11 (CBPL-112)	12 (CBPL-113)	13 (CBPL-114)	14 (CBPL-115)	GW501516
PDBid	5U3Z	5U40	5U41	5U42	5U43	5U44	5U45	5U46
Space group	<i>P 1 2₁ 1</i>							
Unit cell dimensions <i>a, b, c</i> (Å), β (°)	39.43, 94.75, 96.05, 97.68	39.34, 94.75, 95.79, 97.11	39.45, 95.12, 95.79, 96.44	39.66, 95.13, 96.52, 98.04	39.64, 95.01, 96.32, 97.6	39.57, 95.41, 96.18, 97.65	39.53, 95.26, 96.44, 97.56	39.86, 94.14, 96.47, 96.77
Data collection								
Resolution range (Å)	47.59-1.72 (1.75- 1.72)	95.05-2.00 (2.03-2.00)	47.59-1.90 (1.93-1.90)	95.13-1.57 (1.60-1.57)	47.74-1.80 (1.83-1.80)	95.32-2.15 (2.20-2.15)	95.26-1.95 (1.98-1.95)	47.90-2.00 (2.05-2.00)
Observed reflections	411115 (8738)	131605 (2727)	152659 (1550)	270137 (5659)	227730 (3994)	93695 (1375)	193310 (2520)	143826 (1388)
Unique reflections	70808 (3208)	43342 (1423)	47329 (976)	91316 (3774)	64330 (2559)	31224 (1112)	50352 (1833)	38083 (759)
Multiplicity	5.8 (2.7)	3.0 (1.9)	3.2 (1.6)	3.0 (1.5)	3.5 (1.6)	3.0 (1.2)	3.8 (1.4)	3.8 (1.8)
Completeness (%)	95.7 (88.4)	91.9 (61.5)	85.5 (35.9)	92.5 (77.7)	98.3 (79.9)	81.0 (44.8)	97.6 (70.7)	79.6 (23.7)
Mean I/sigma(I)	9.8 (0.8)	30.9 (1.0)	10.7 (0.8)	61.8	40.9	21.4 (0.6)	7.4 (1.0)	10.9 (1.7)
CC(1/2)	0.997 (0.390)	0.975 (0.278)	0.984 (0.547)	0.995 (0.497)	0.992 (0.662)	0.983 (0.409)	0.994 (0.497)	0.996 (0.790)
Data refinement								
Wilson B-factor	25.64	15.00	24.77	21.14	23.90	31.42	25.28	25.81
R-work/ R-free	0.1742/0.2124	0.1940/0.2293	0.2097/0.2693	0.1767/0.2164	0.1863/0.2387	0.1991/0.2526	0.1951/0.2419	0.1758/0.2228
RMSD (bonds)	0.011	0.003	0.003	0.012	0.012	0.002	0.004	0.003
RMSD (angles)	1.32	0.73	0.58	1.30	1.15	0.50	0.81	0.72
Ramachandran favored/allowed/ outliers (%)	98/1.9/0	98/2.3/0	98/1.7/0	98/1.7/0	98/1.9/0	98/1.6/0	99/1.3/0	99/1.1/0
Clashscore	1.41	0.45	0.45	1.73	2.21	1.62	0.45	0.56
Average B-factor	41.07	26.13	33.51	35.24	37.79	49.08	38.81	38.58

Statistics for the highest-resolution shell are shown in parentheses.

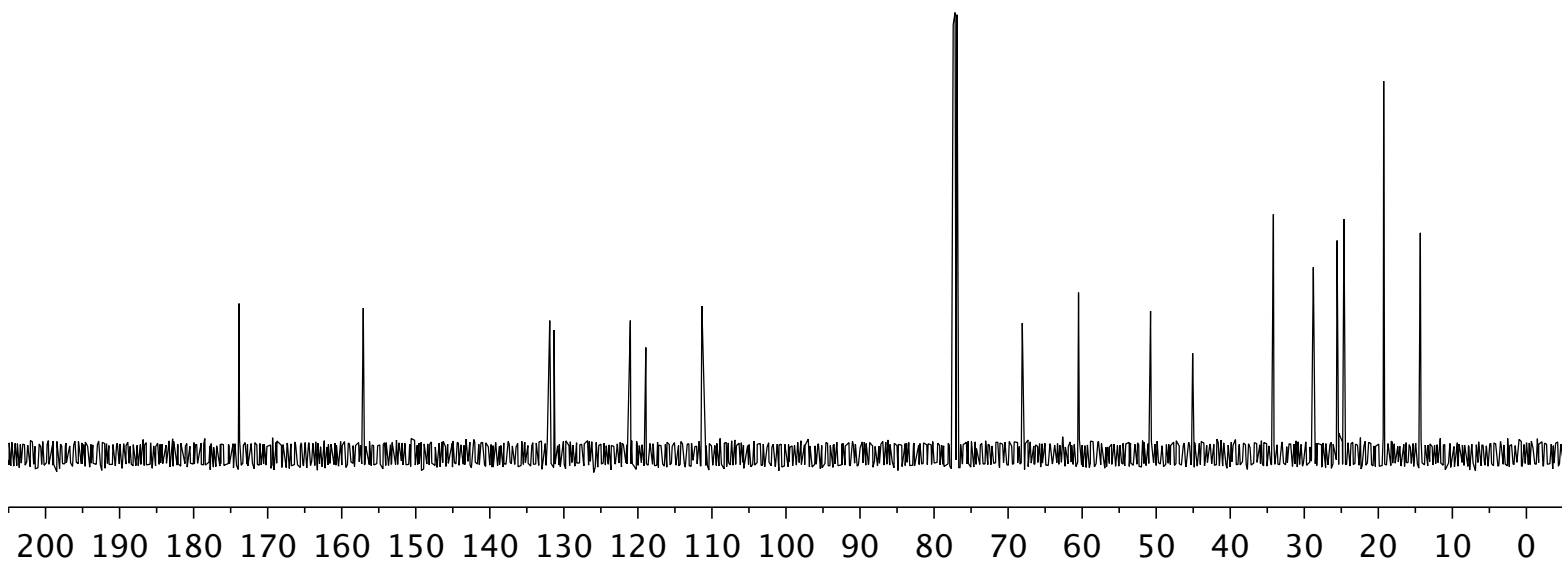
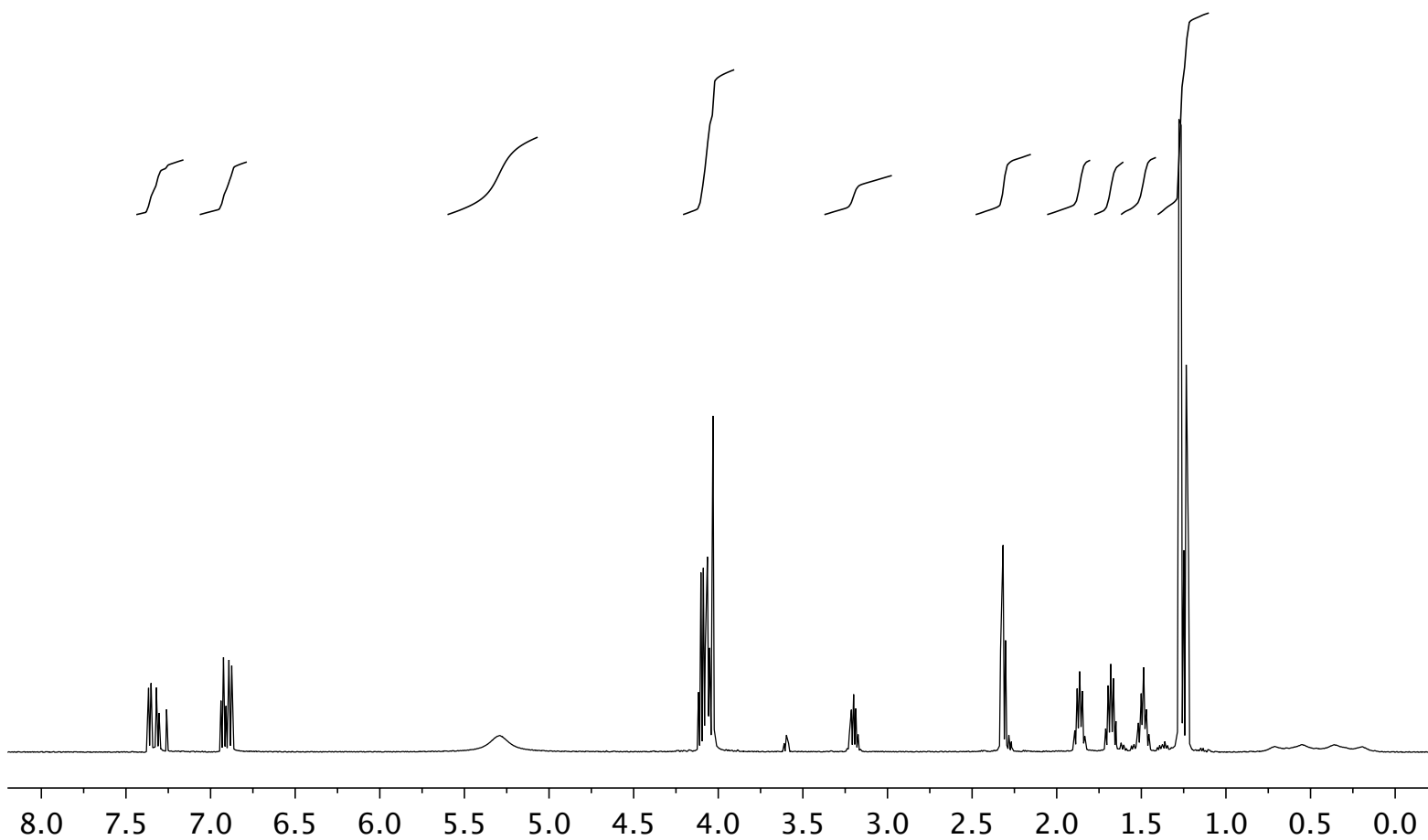
Table S3. Correlation between ligands' tail structures and H2'-H3 conformations in the ligand-bound hPPAR δ -LBD structures.

Distal group of ligand tail (R ₂)	Compound	Torsion angles between ring B and C in °		W228 conformation (Chi1/Chi2 angles in °)	
		chain A	chain B	chain A	chain B
	2	-4.3	-7.7	non-flip (-67.3/-80.3) flip (-50.4/81.3)	non-flip (-73.3/-76.8)
	5	-11.7	(no ligand)	non-flip (-74.2/-72.2)	disordered
	9	5.0	-1.3	non-flip (-67.4/-73.6)	non-flip (-71.6/-71.5)
	3	-7.6	-12.7	non-flip (-66.4/-80.1) flip (-60.9/84.1)	flip (-51.7/81.1)
	6	-14.7	-11.2	non-flip (-87.2/-69.0) flip (-53.0/81.7)	non-flip (-69.6/-80.0) flip (-49.8/78.4)
	10	-7.9	-7.4	flip (-56.3/84.5)	flip (-55.0/81.3)
	15	-1.7	-0.2	non-flip (-66.0/-82.4)	non-flip (-70.5/-83.1) flip (-60.1/82.6)
	4	-18.2	-13.4	flip (-53.6/84.2)	flip (-51.8/80.6)
	16	-15.3	-1.65	flip (-57.7/77.3)	flip (-59.2/81.5)
	1	-24.3	-25.6	flip (-57.2/83.1)	flip (-53.8/85.1)
	7	-20.5	-18.4	flip (-49.2/79.4)	flip (-60.8/87.5)
	8	-12.7	-8.1	non-flip (-70.5/-78.7)	disordered
	11	-14.0	-18.8	flip (-62.8/90.2)	flip (-60.4/88.9)
	12	-18.9	-15.9	flip (-58.0/89.7)	flip (-59.3/89.5)
	13	-25.8	-26.0	disordered	disordered
	14	-9.2	-20.4	flip (-58.6/84.9)	flip (-58.2/88.1)
	GW501516	(no B-C ring)	(no B-C ring)	flip (-55.5/82.2)	flip (-55.5/84.4)
	GW0742 (PDB: 3TKM) (37)	(no B-C ring)	(no B-C ring)	flip (-56.4/86.9)	(no chain B)
	(PDB:2XYX) (44)	(no B-C ring)	(no B-C ring)	flip (-58.2/82.2)	flip (-55.1/85.9)
	(PDB:2XYW) (44)	(no B-C ring)	(no B-C ring)	flip (-54.0/98.5)	flip (-54.0/98.5)
	(PDB:2XYJ) (44)	(no B-C ring)	(no B-C ring)	flip (-51.1/69.7)	non-flip (-94.0/-57.1)

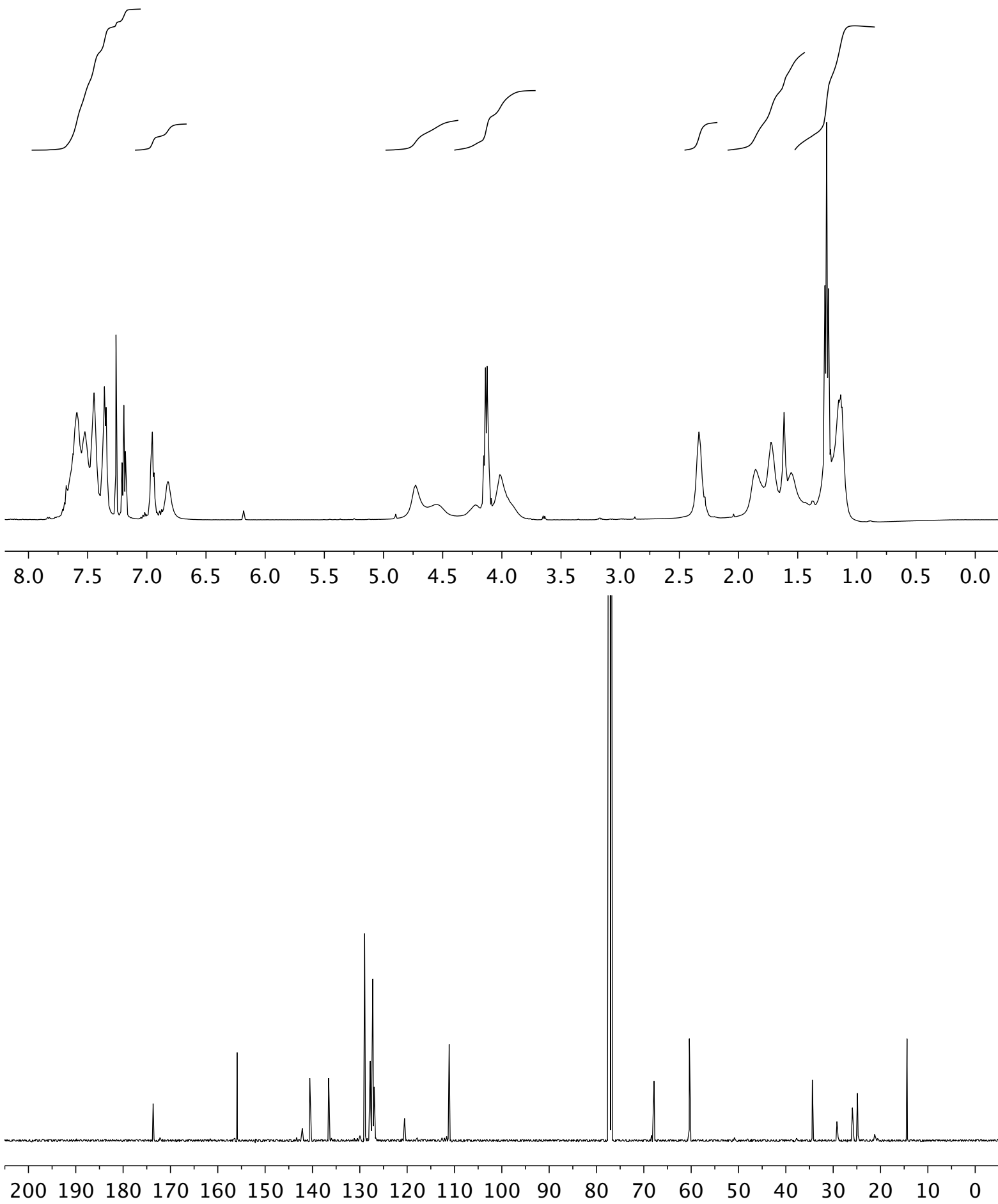
$^1\text{H-NMR}$ (500 MHz) and $^{13}\text{C-NMR}$ (125 MHz) spectra of aldehyde **S1** in CDCl_3



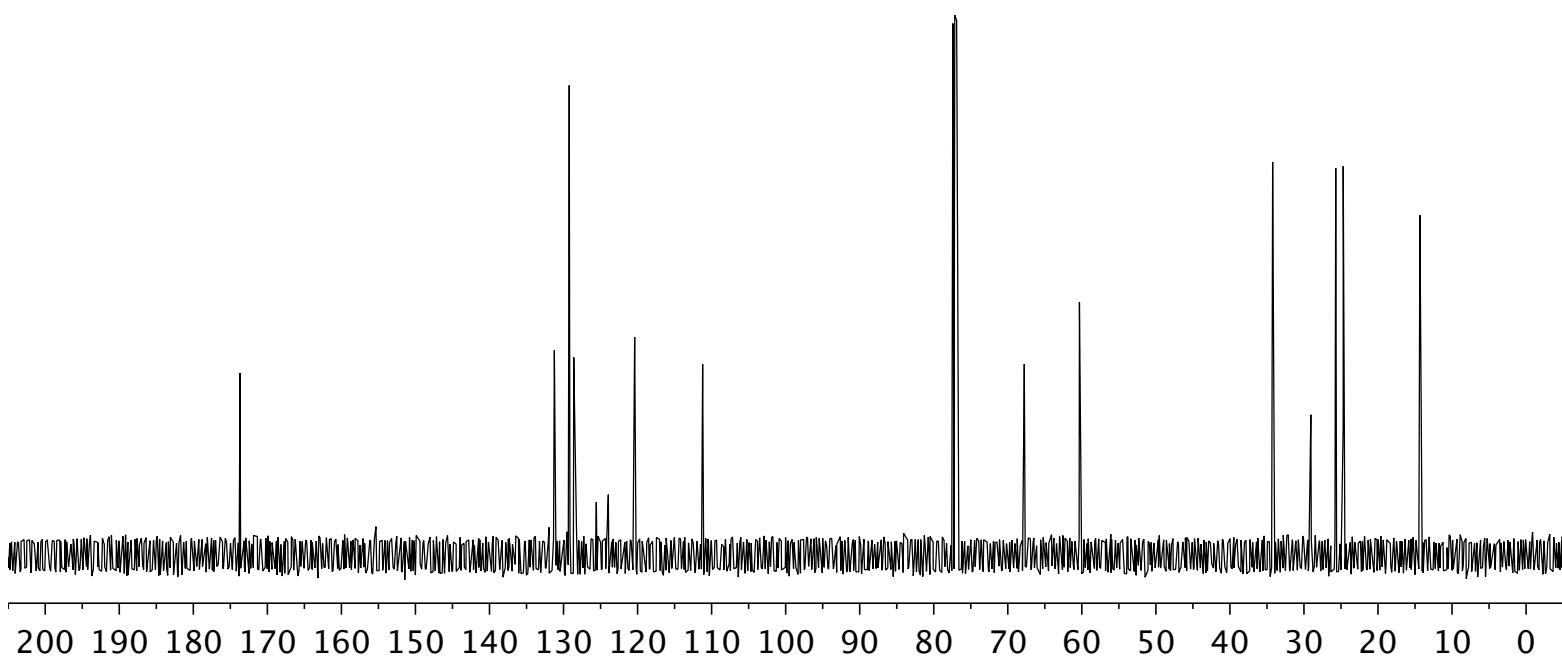
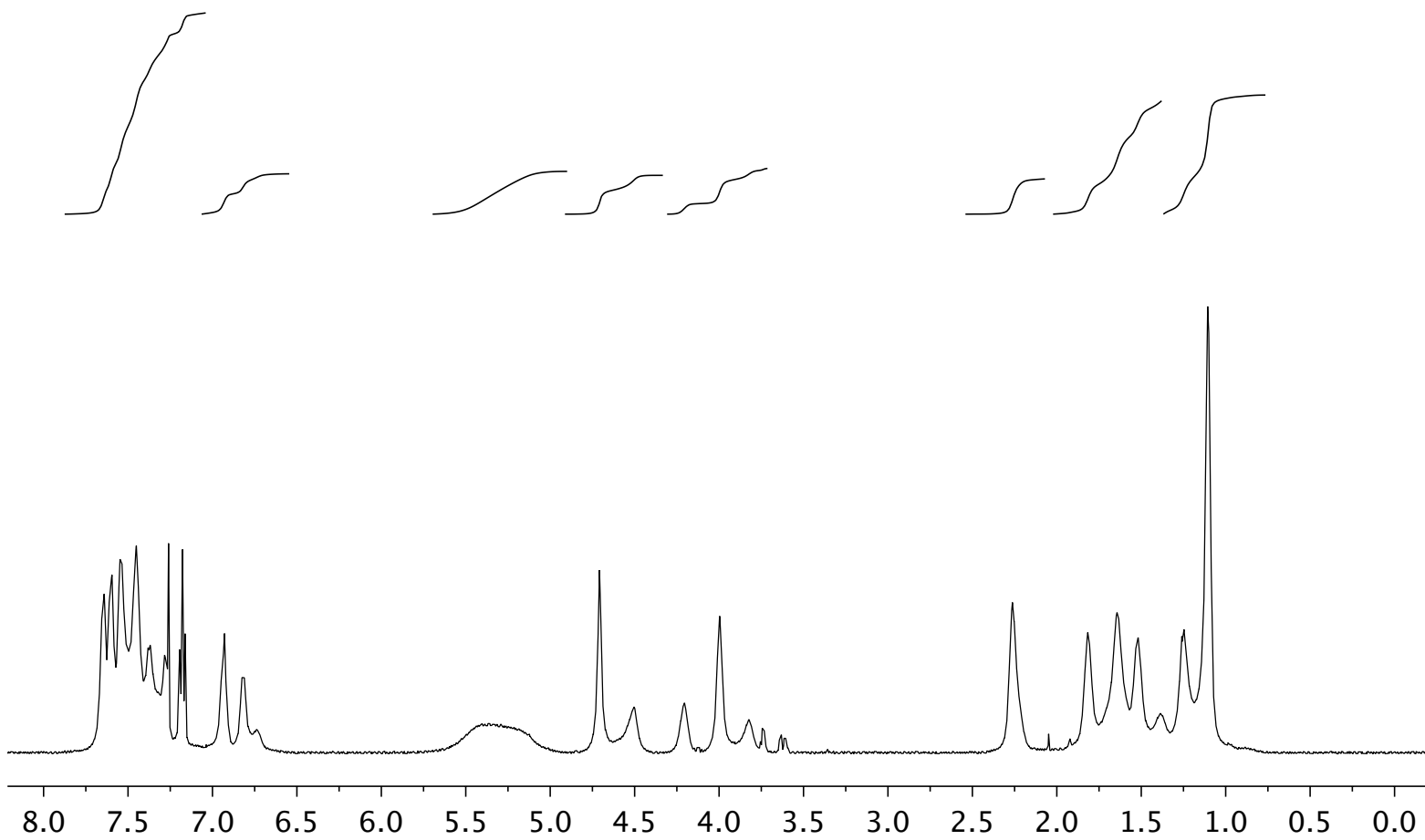
$^1\text{H-NMR}$ (500 MHz) and $^{13}\text{C-NMR}$ (125 MHz) spectra of amine **S3** in CDCl_3



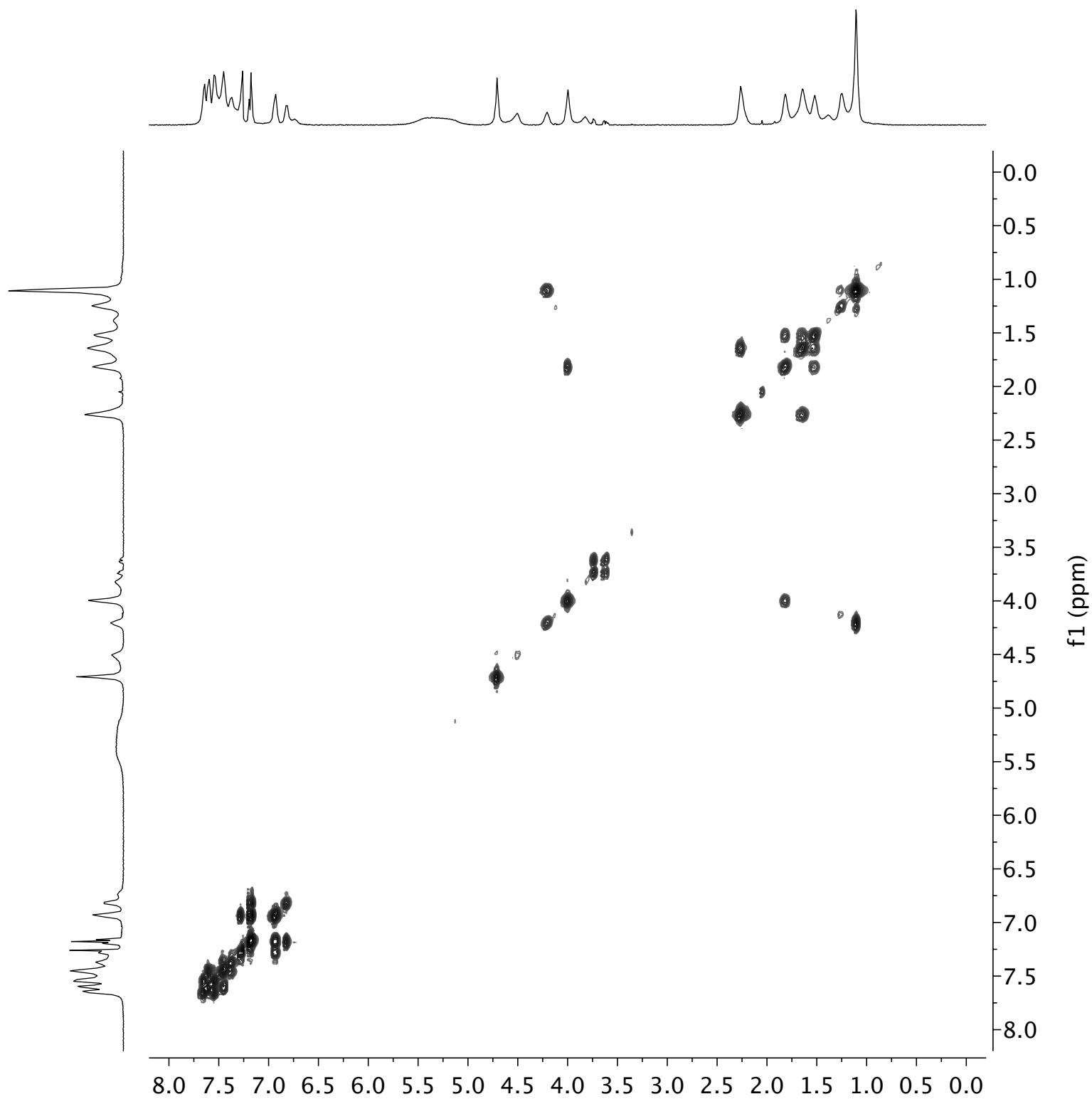
^1H -NMR (500 MHz) and ^{13}C -NMR (125 MHz) spectra of ester **S4** in CDCl_3



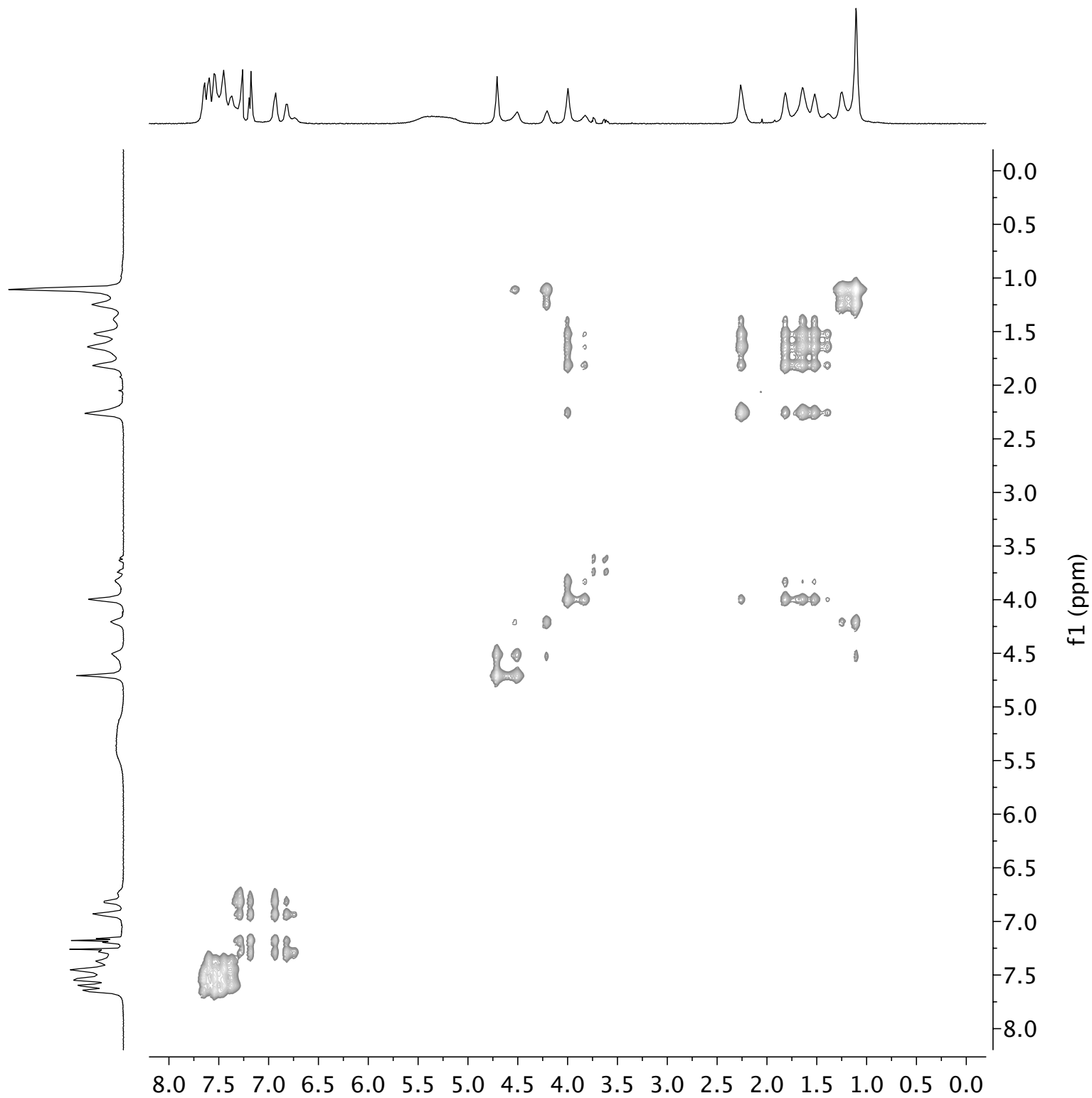
^1H -NMR (500 MHz) and ^{13}C -NMR (125 MHz) spectra of compound **1** in CDCl_3



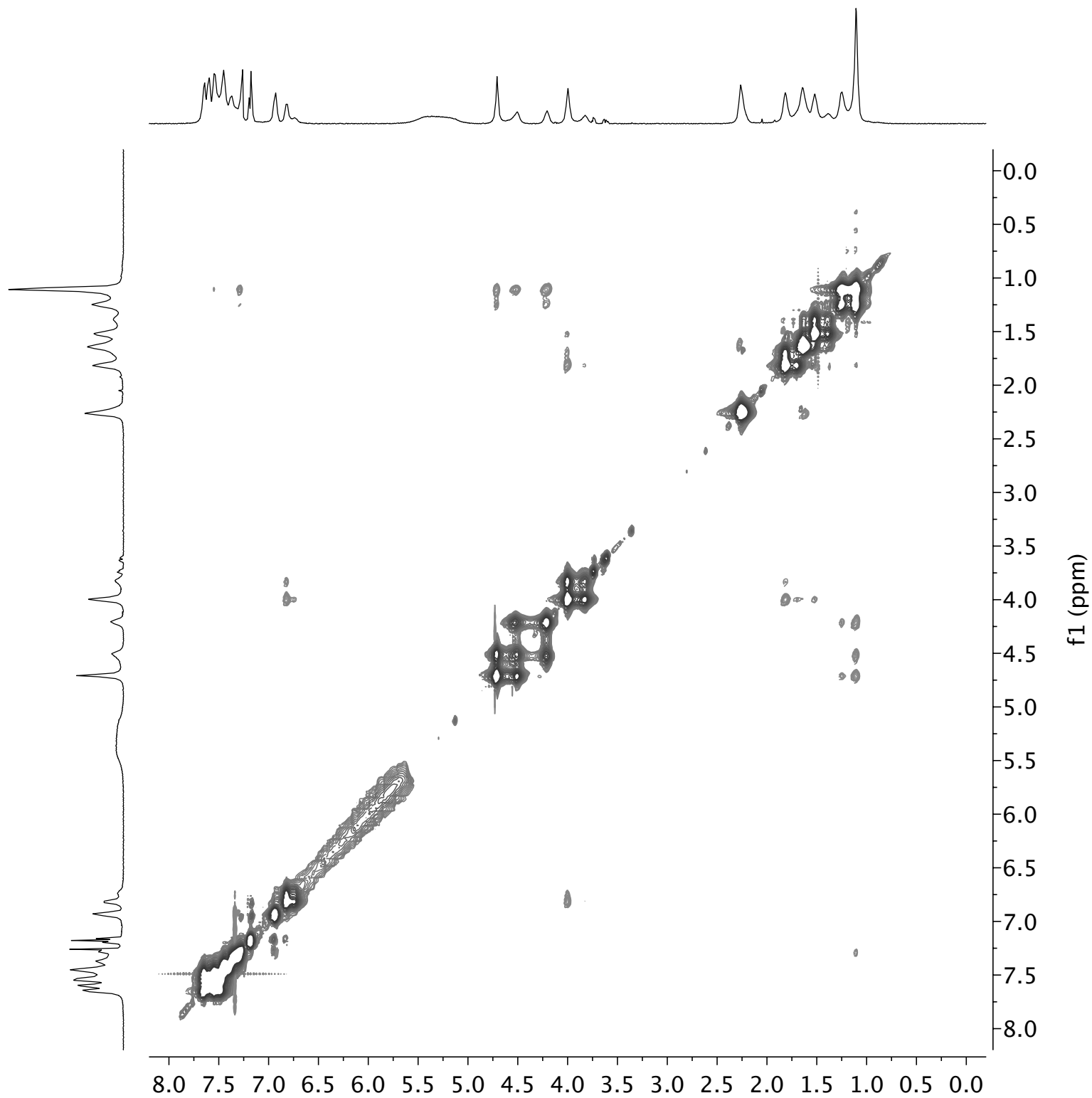
^1H , ^1H -gCOSY (500 MHz) spectra of compound **1** in CDCl_3



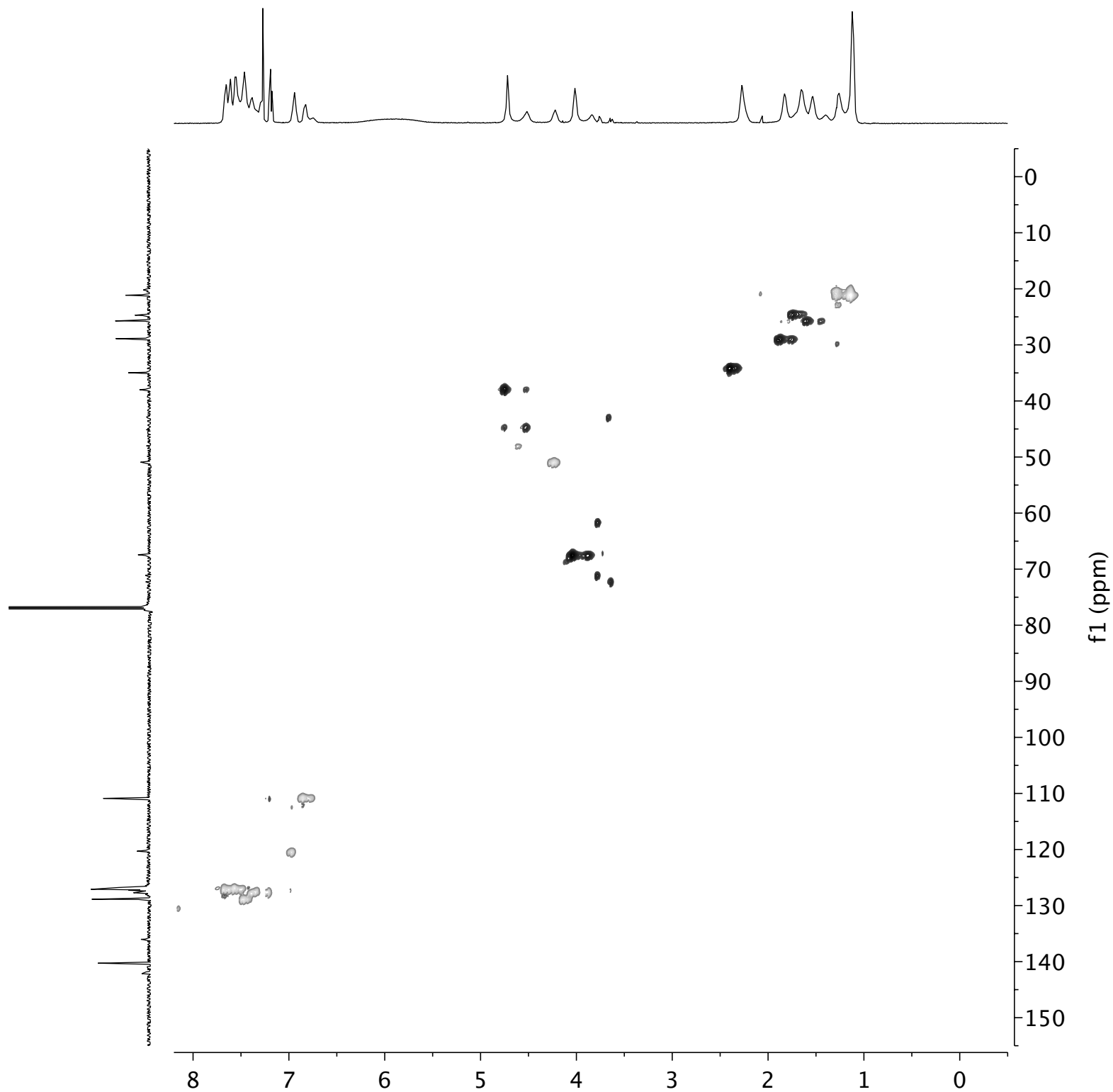
$^1\text{H}, ^1\text{H}$ -TOCSY (500 MHz) spectra of compound **1** in CDCl_3



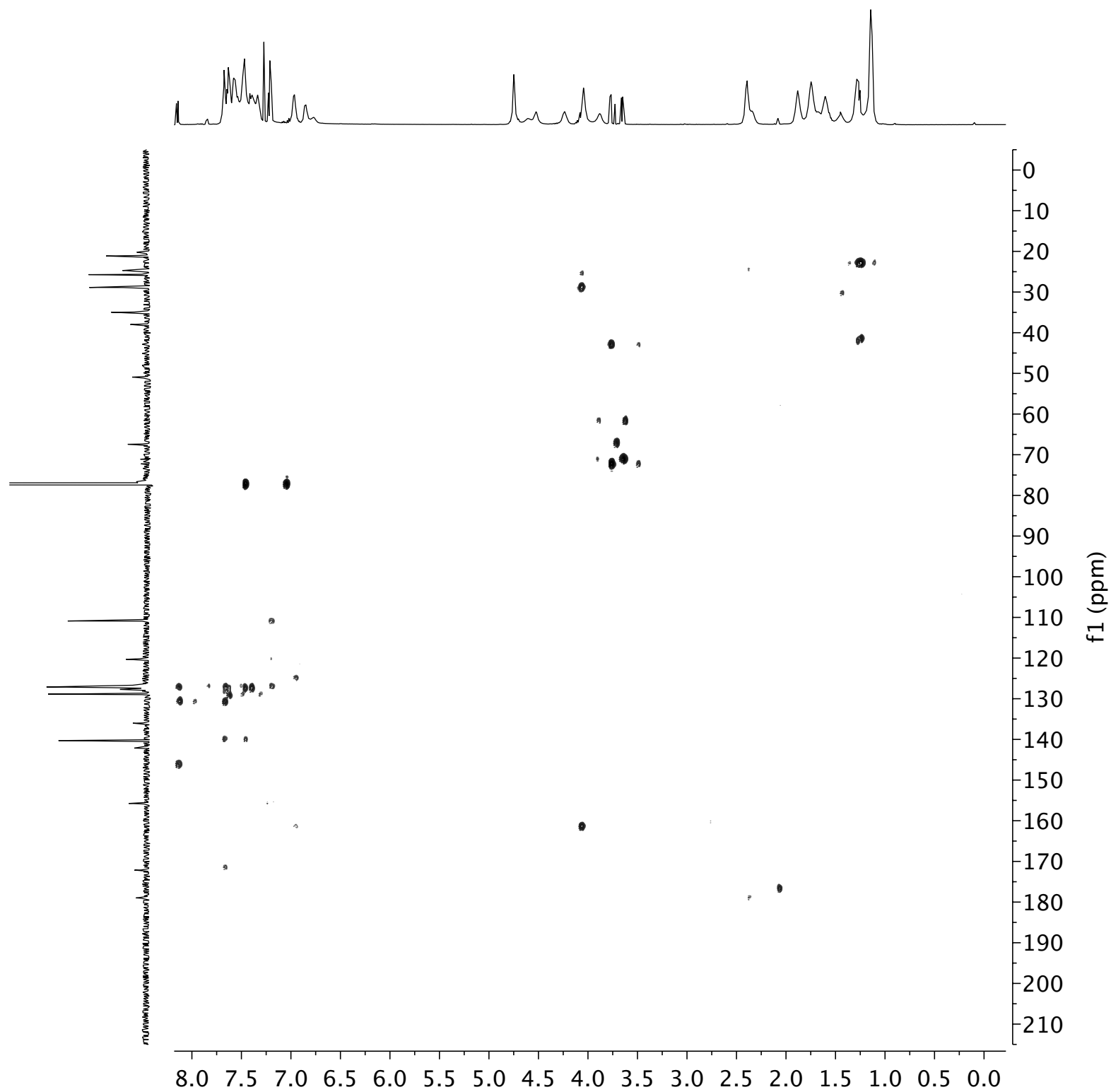
$^1\text{H}, ^1\text{H}$ -NOESY (500 MHz) spectra of compound **1** in CDCl_3



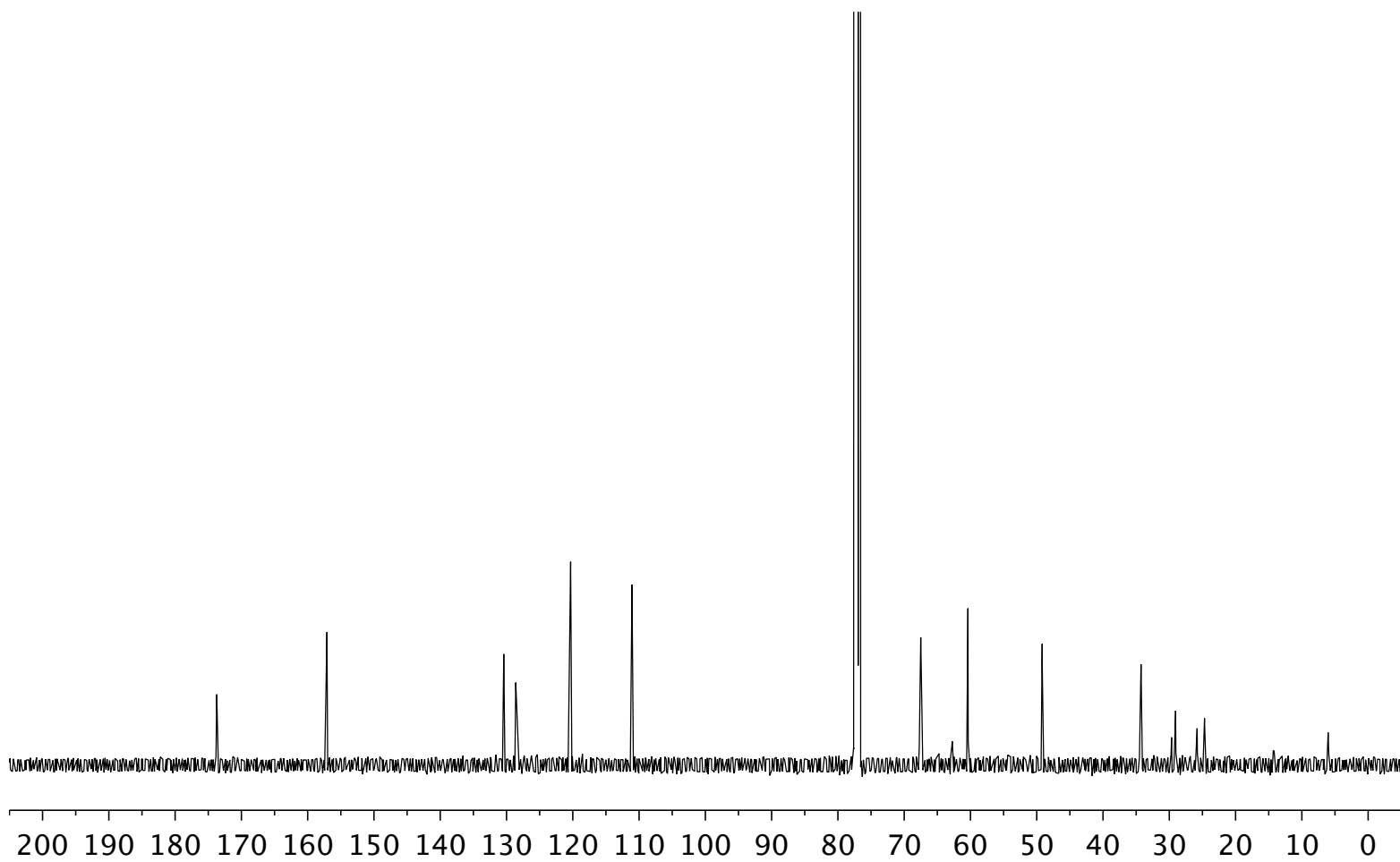
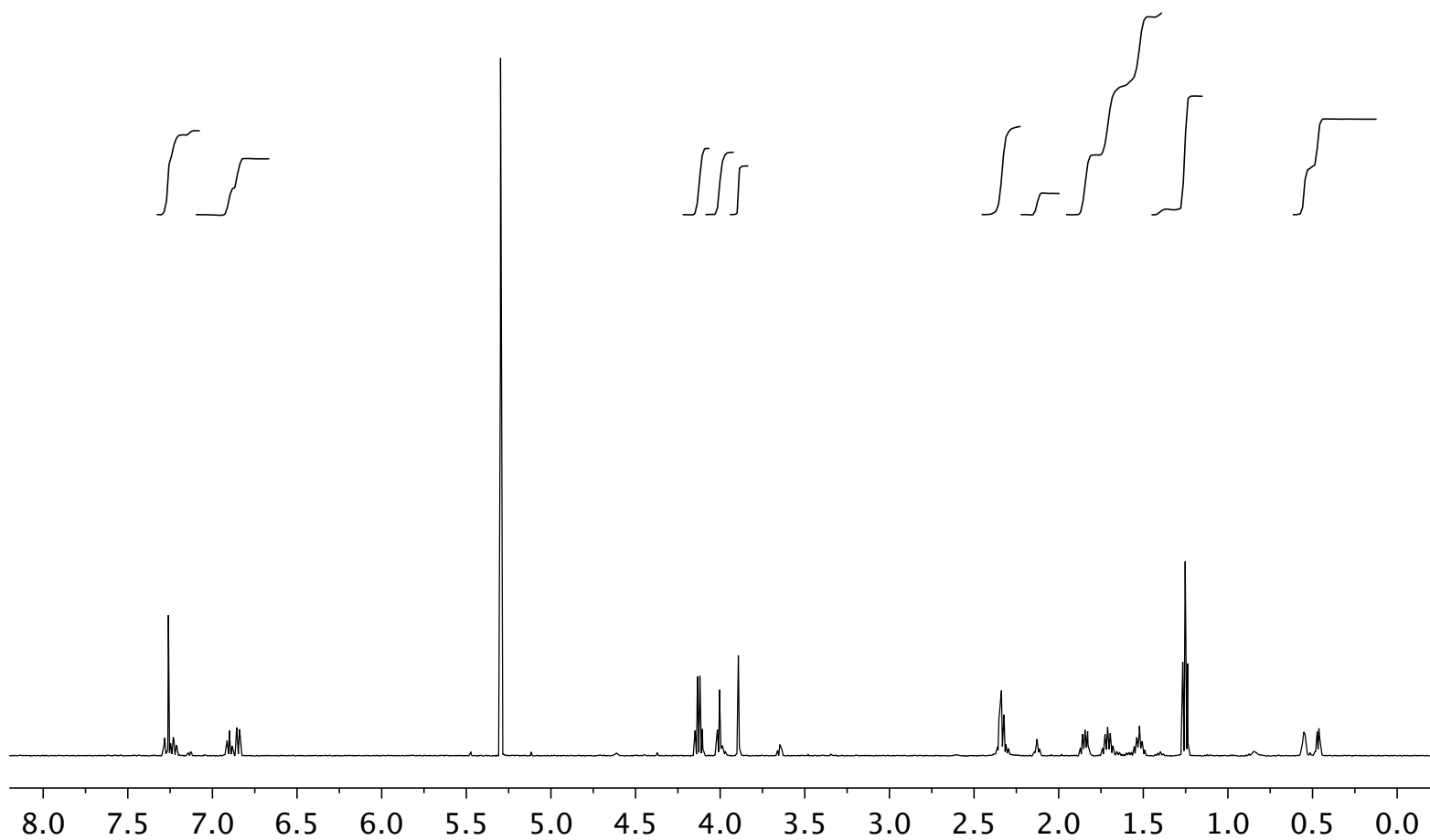
^1H , ^{13}C -HSQC (500 MHz) spectra of compound **1** in CDCl_3



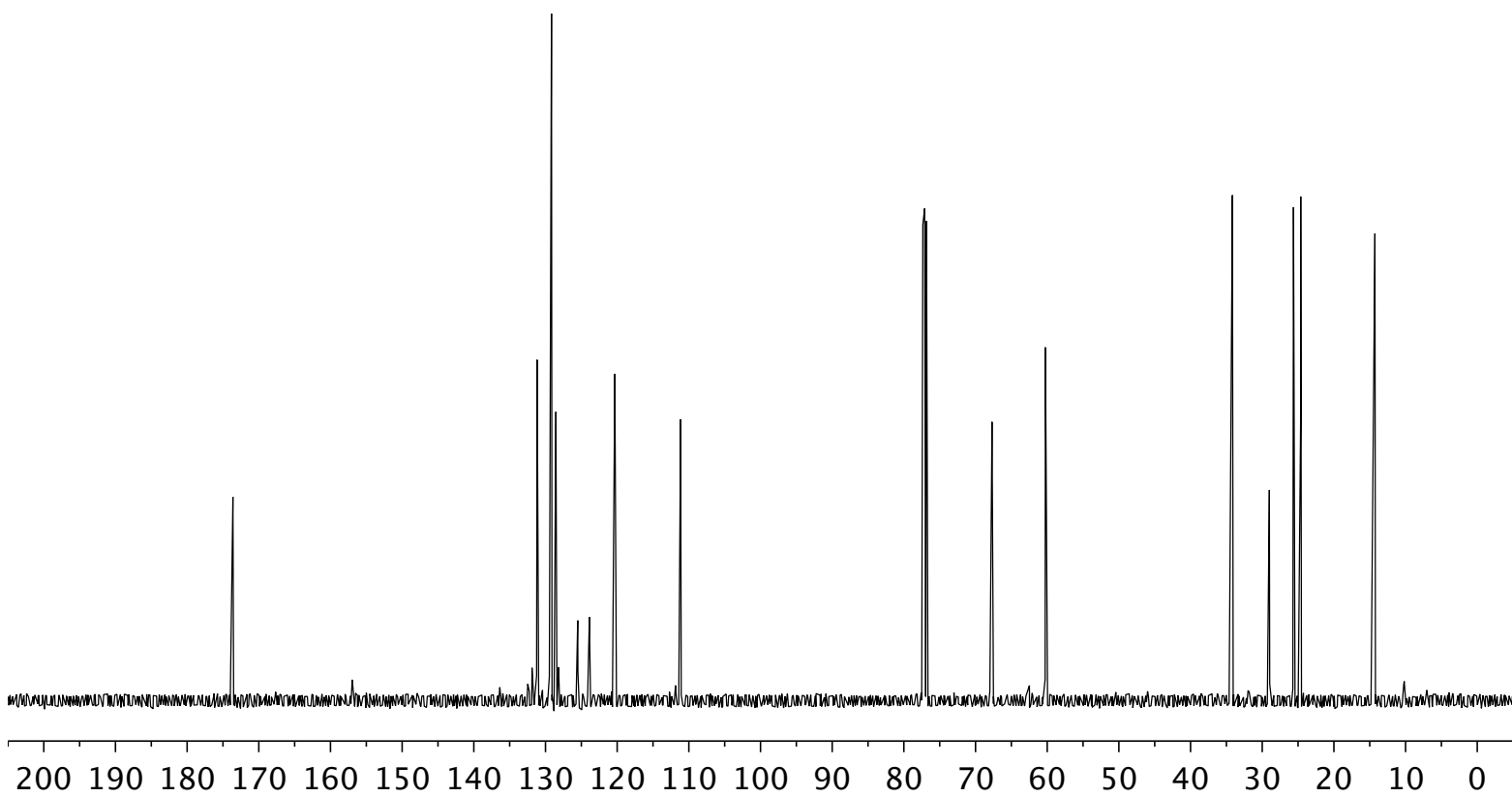
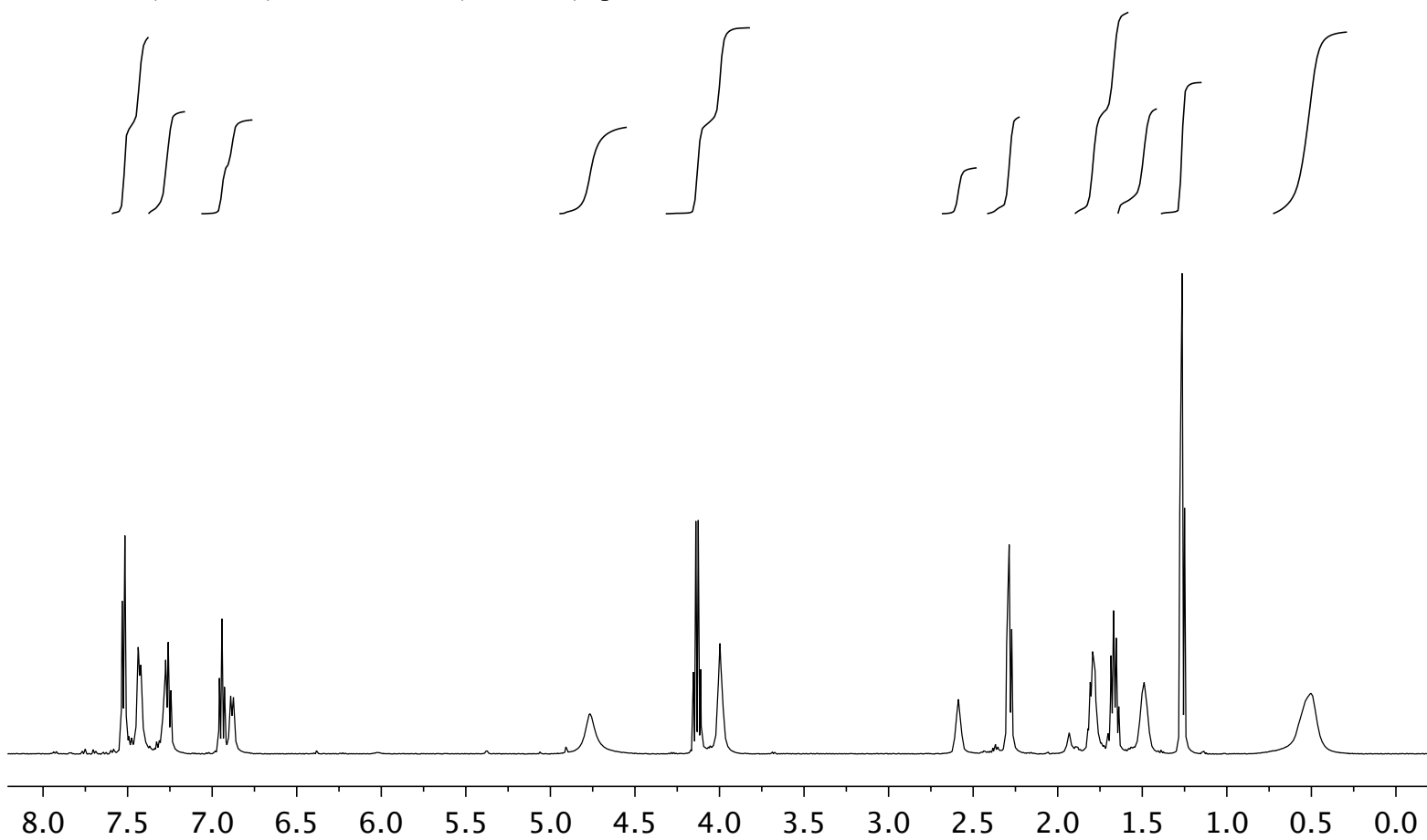
^1H , ^{13}C -HMBC (500 MHz) spectra of compound **1** in CDCl_3



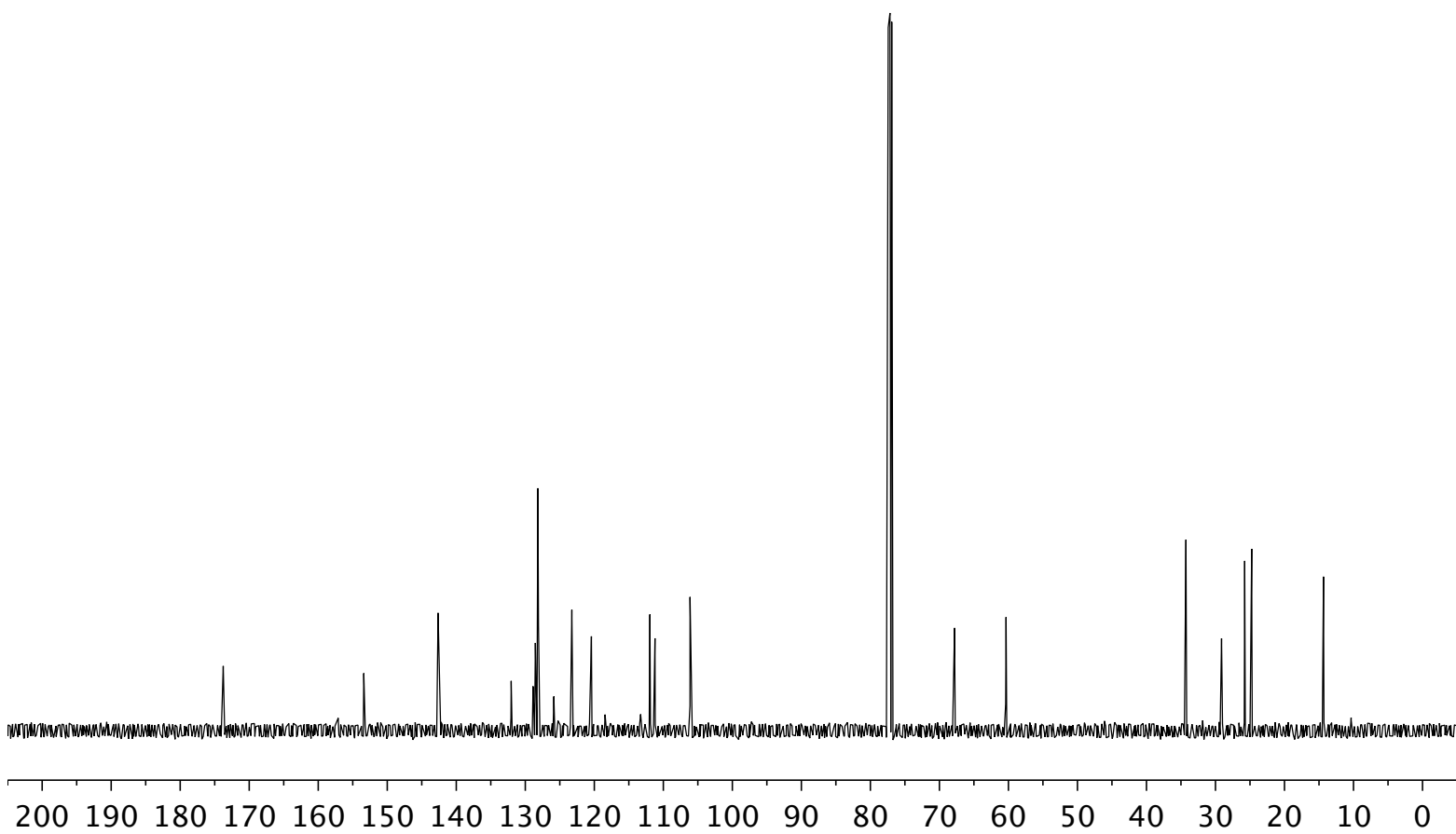
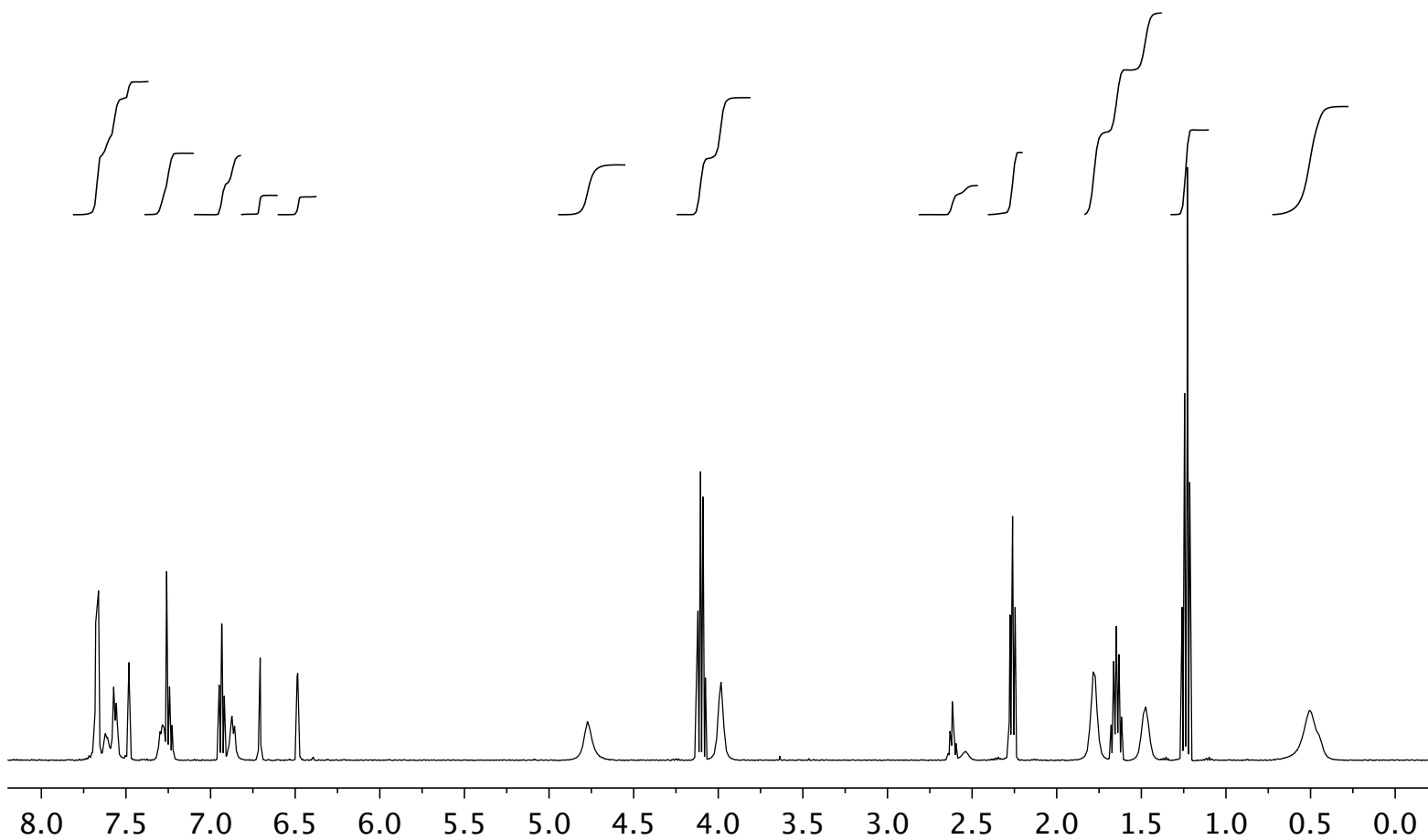
$^1\text{H-NMR}$ (500 MHz) and $^{13}\text{C-NMR}$ (125 MHz) spectra of amine **S6** in CDCl_3



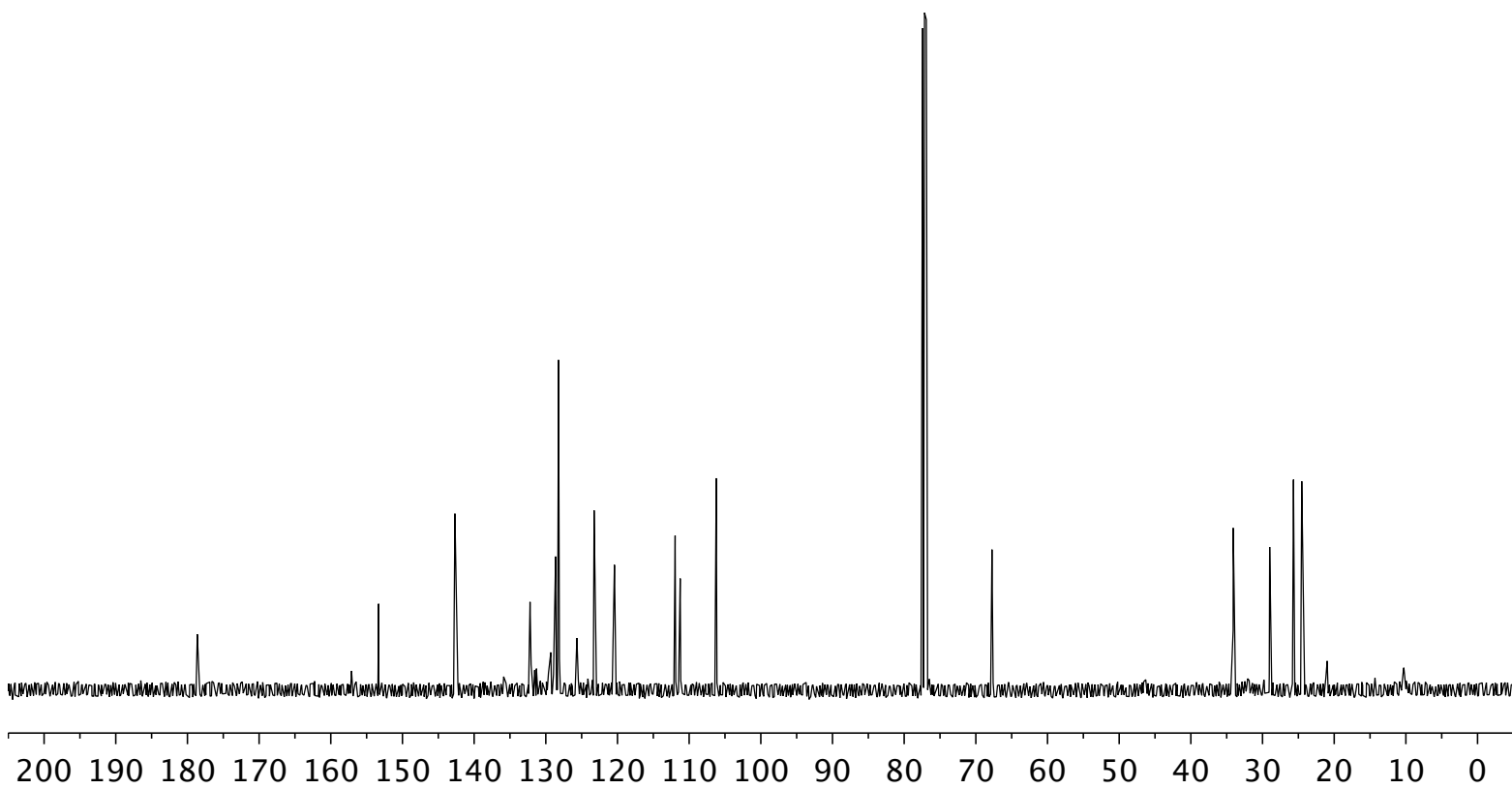
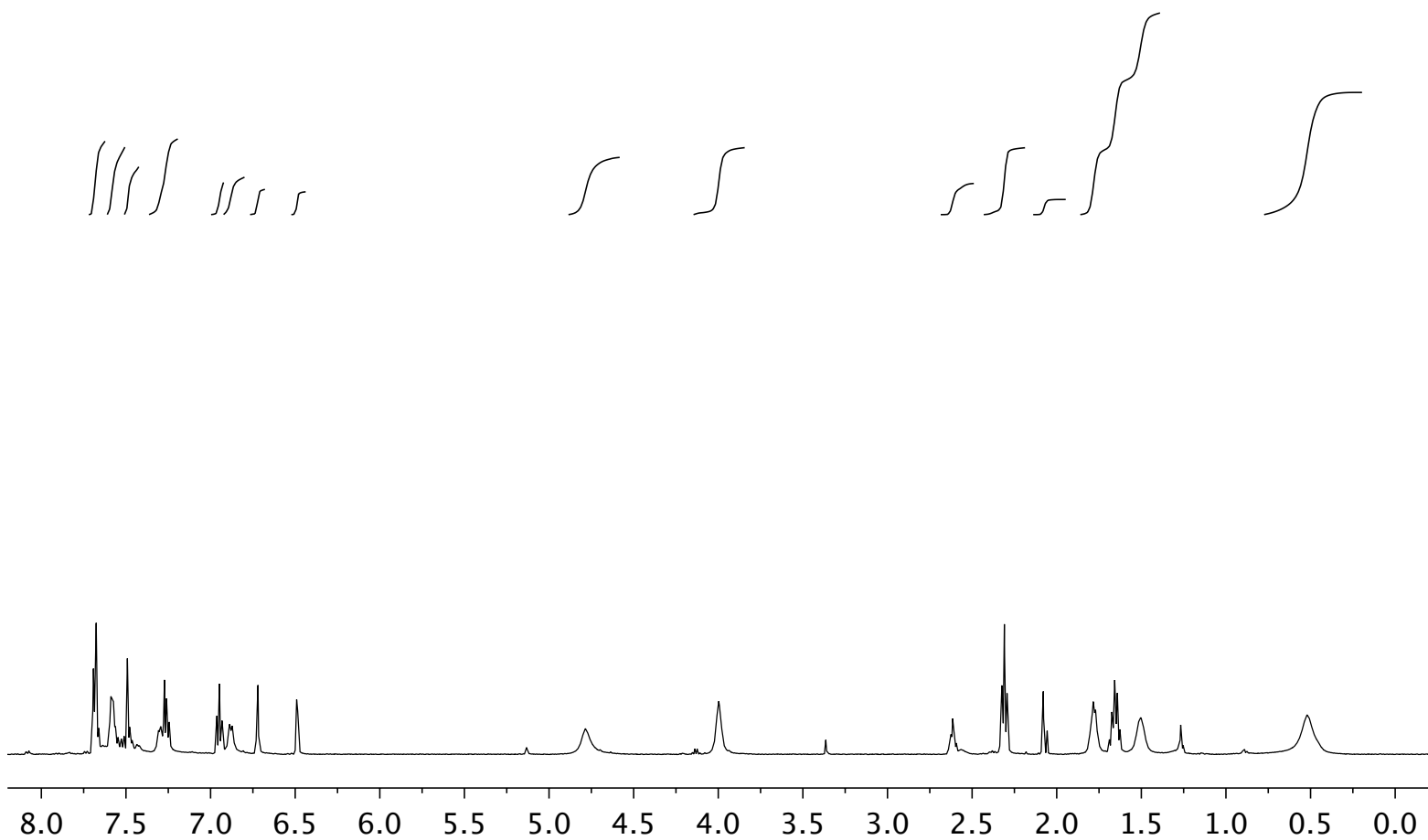
^1H -NMR (500 MHz) and ^{13}C -NMR (125 MHz) spectra of amide **S7** in CDCl_3



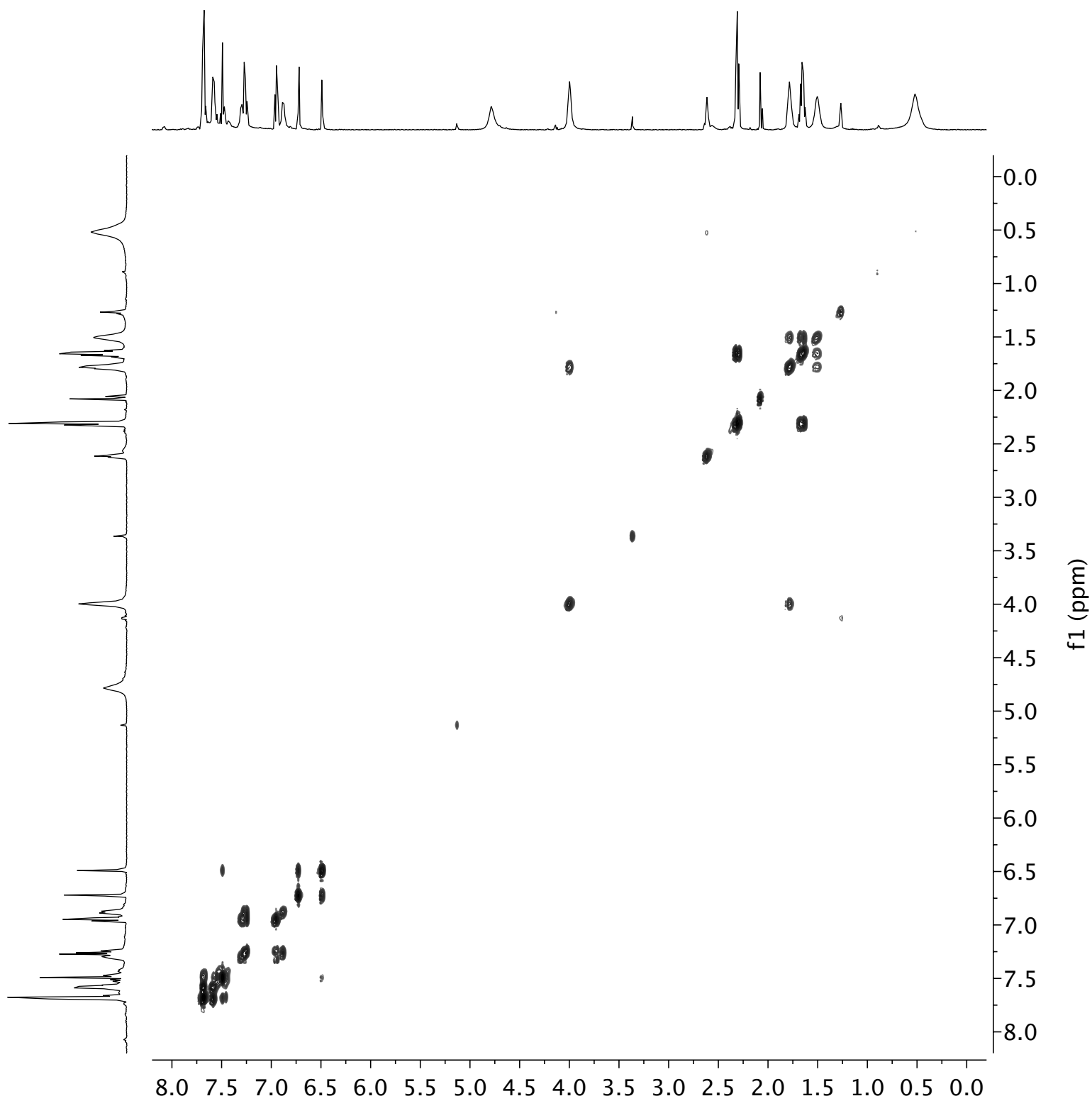
$^1\text{H-NMR}$ (500 MHz) and $^{13}\text{C-NMR}$ (125 MHz) spectra of ester **S8** in CDCl_3



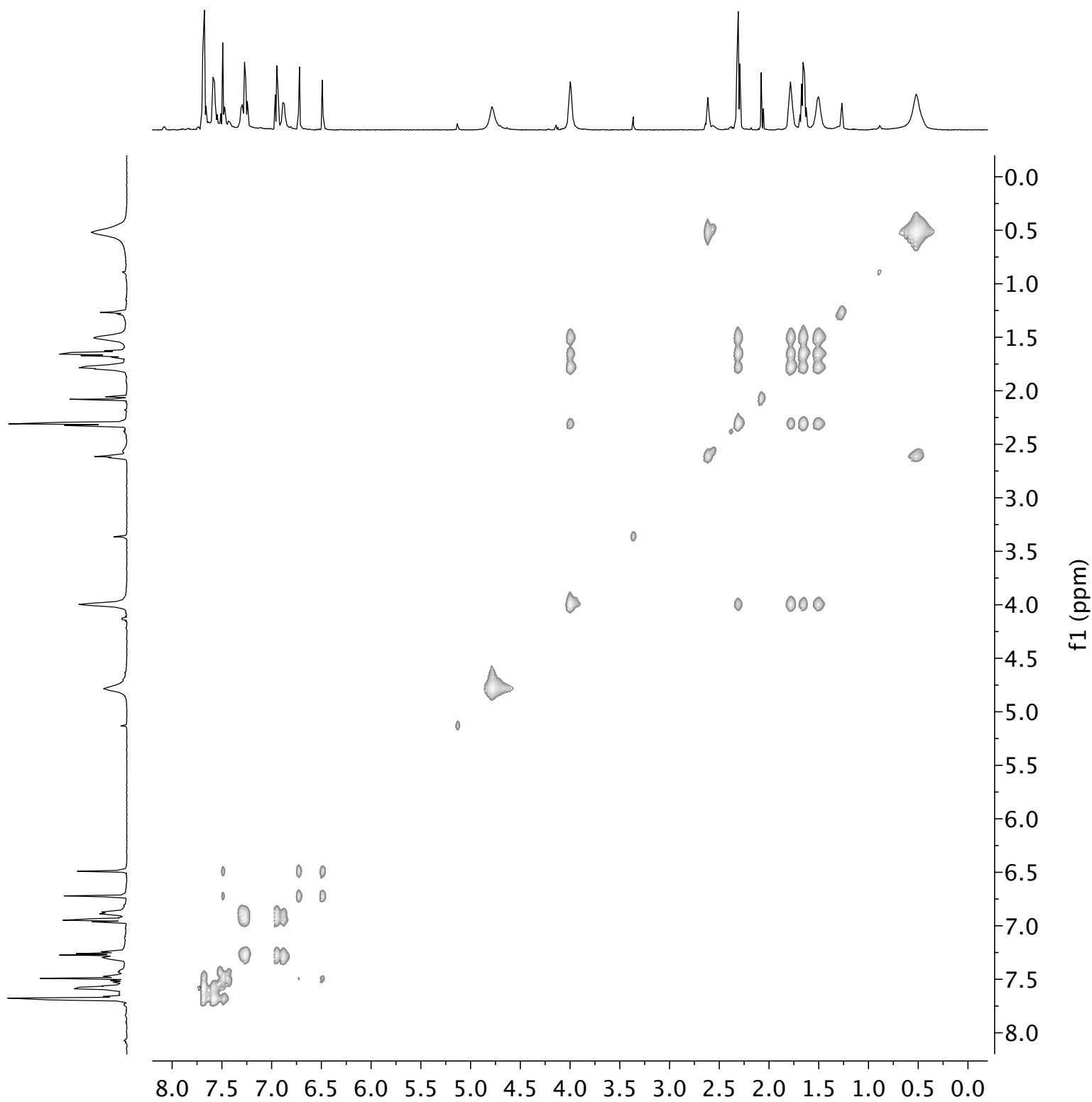
$^1\text{H-NMR}$ (500 MHz) and $^{13}\text{C-NMR}$ (125 MHz) spectra of compound **9** in CDCl_3



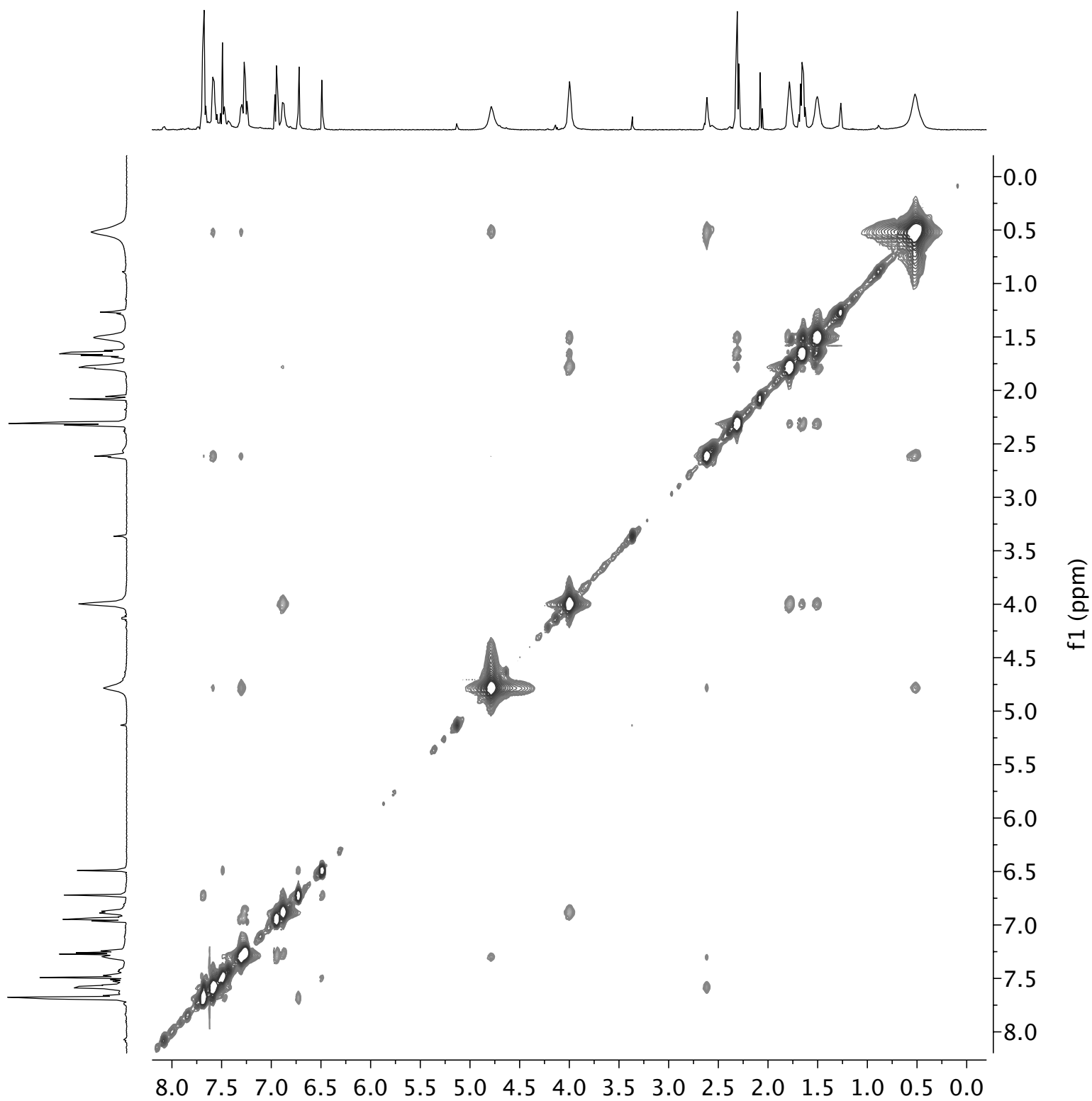
^1H , ^1H -gCOSY (500 MHz) spectra of compound **9** in CDCl_3



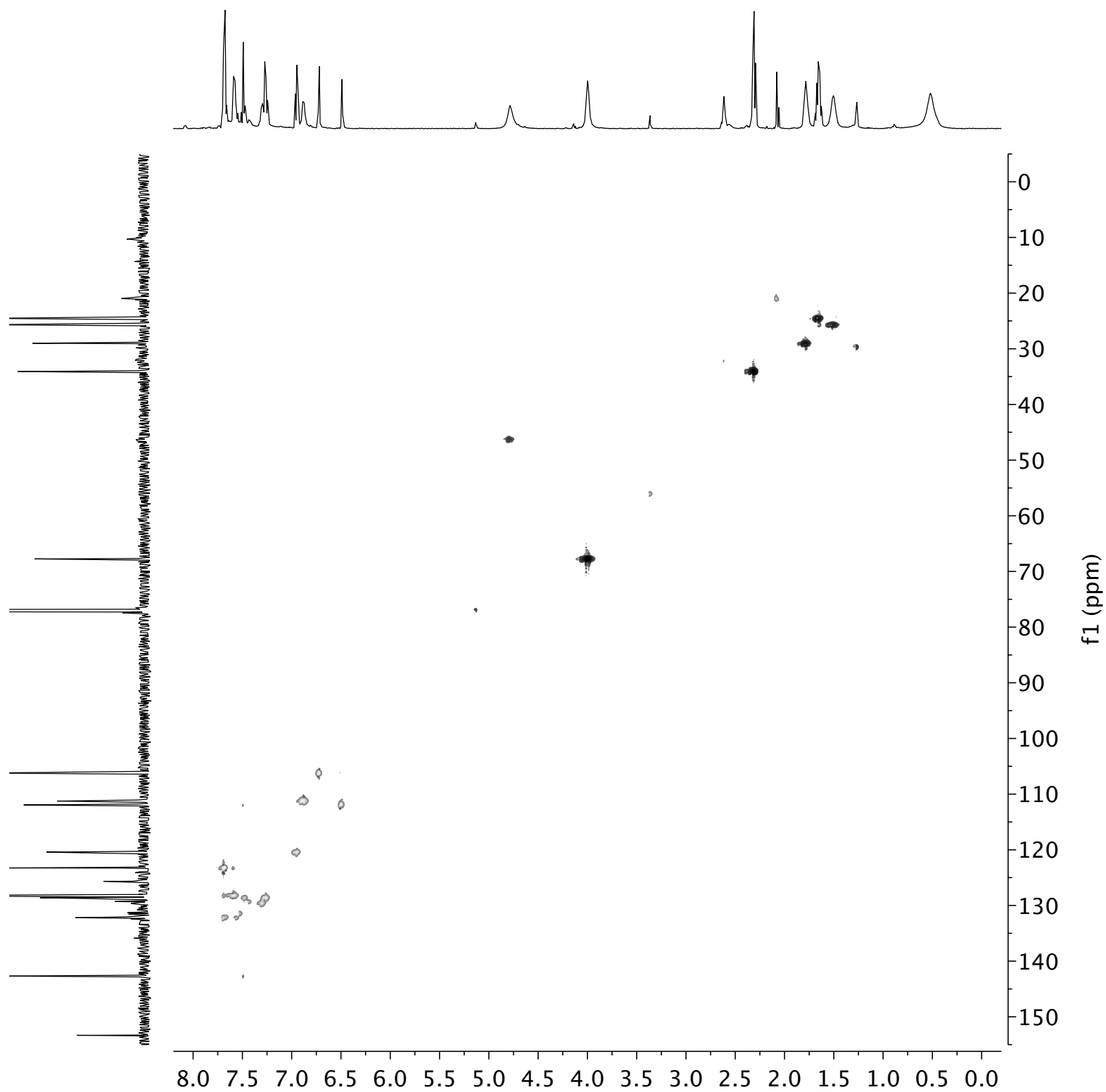
^1H , ^1H -TOCSY (500 MHz) spectra of compound **9** in CDCl_3



^1H , ^1H -NOESY (500 MHz) spectra of compound **9** in CDCl_3



$^1\text{H}, ^{13}\text{C}$ -HSQC (500 MHz) spectra of compound **9** in CDCl_3



^1H , ^{13}C -HMBC (500 MHz) spectra of compound **9** in CDCl_3

